Title
Phase-Sensitive Dynamic Filtering with Time-Varying Transmission Line Filters

Author
Chen, Sean Ching Chuan

Publication Date
2023

Peer reviewed|Thesis/dissertation

UNIVERSITY OF CALIFORNIA

Los Angeles

Phase-Sensitive Dynamic Filtering with Time-Varying Transmission Line Filters

A thesis submitted in partial satisfaction

of the requirements for the degree Master of Science

in Electrical and Computer Engineering

by

Sean Ching Chuan Chen

2023

ABSTRACT OF THE THESIS

Modeling Phase-Sensitive Dynamic Filtering with Time-Varying Transmission Line Filters

by

Sean Ching Chuan Chen

Master of Science in Electrical and Computer Engineering

University of California, Los Angeles, 2023

Professor Yuanxun Wang, Chair

Bandpass filters play an integral role in virtually all communications systems. However, their constraints often clash with the increasing need for frequency and bandwidth resources. With this problem arises the need to be able to tune filters in real time. Dynamic filters can be used to address some of the traditional concerns regarding spectrum utilization and rapid frequency/phase shifts. These are filters that can be tuned in real time, with switching speeds faster than the symbol rate of a signal, and time constants longer than the symbol periods, enabling fast switching with negligible charge decay/pulsing. In this thesis, we propose IIR filters to provide an adequate basis in demonstrating the theory behind the dynamic filters, and the Time-Varying Transmission Line (TVTL) as an adequate candidate for realizing these filters. The theory of the dynamic bandpass filters is explored with a potential application utilizing such filters in the front end of a full-duplex communications system.

The thesis of Sean Ching Chuan Chen is approved.

Danijela Cabric

Gregory J. Pottie

Yuanxun Wang, Committee Chair

University of California, Los Angeles

2023

TABLE OF CONTENTS

LIST OF FIGURES

ACKNOLEDGEMENTS

I would like to thank my advisor, Professor Yuanxun Wang, for his professional guidance, remarks, and support for this work. His passion for research and exploring new topics encourages me to push on even amidst the discouragement of feeling lost in my work. I appreciate his willingness to always make time to discuss my research with me and to offer advice throughout the process.

Additionally, I would like to thank Professor Gregory Pottie and Professor Danijela Cabric for their patience in reading and approving this work.

I am very grateful for my lab mates, Jerry Li, Kamal Bahkta, Nancy Gao, and Lap Yeung for being exemplar older role models and for their help and meaningful discussions during these past couple of years.

A huge thanks to my church friends who have kept me grounded and have always been willing to lend a listening ear when I need people to talk with.

I also want to thank my family. Starting with my two siblings – Isabelle and Daniel – for keeping me sane throughout the tumultuous seasons in my life and reminding me that life is more than just doing work. I want to thank both of my Uncles for their mentorship, and my Grandma for supporting me with the best food. I especially want to thank my mother and father, for their unconditional love and support throughout my entire life. Without their support, encouragement, and guidance, I would not be able to pursue this opportunity.

Lastly, I would like to thank God for being with me every step in this journey, and being the one I can lean on and trust regardless of my situation.

CHAPTER 1

Introduction

Effectively all communication systems rely on bandpass filters, but their limitations can clash with the increasing need for frequency and bandwidth resources. Therefore, there is a need to adjust these filters in real-time to resolve this issue. For example, a bandpass filter with a narrow bandwidth produces sharper frequency selectivity which is useful for signals in close frequency proximity to each other; however, the phase and waveform of such modulated signals are often warped and consequentially not properly conserved. Additionally, the conventional tunable bandpass filters are typically inadequate for real-time switching due to their slow tuning speeds and inability to track phase and frequency changes in real time.

1.1 Background and Motivation

Fundamentally, there is a direct inverse relation between the settling time of a filter and its Q-factor. First, the relation between bandwidth and a filter's time constant can be given by the following equation:

$$\Delta f \cdot \tau_f = a \tag{1.1.1}$$

Where Δf is the 3-dB passband of the filter, τ_f is the time constant, and a is the proportionality constant (often chosen to be 0.35 when modeled by RC circuits). The Q factor of the filter is given by the following equation:

$$Q = \frac{f_c}{\Delta f} \tag{1.1.2}$$

Where f_c is the center passband of the filter. From this, it can be observed that as the bandwidth of a filter increases, the time constant decreases, and the Q factor decreases – thus indicating a limit in time it takes a filter to settle given its operating bandwidth. The higher the Q, the longer the settling time. From a communications perspective, the filter is typically deemed operational when it has fully "settled" (time constant reached). For fixed bandpass filtering, this does not pose to be a critical concern, as it is merely a fixed latency which takes place in the initial portion filtering, which does not have any significant drawback. However, for applications utilizing real-time passband switching, this is a cause of concern as this bandwidth limit introduces periods of inactivity due to settling time between switches.

1.2 Traditional Bandpass Filtering

The traditional fixed-filter approach is to design a bandpass filter which encapsulates the entirety of the spectrum in which the signal is located. This approach is straightforward and easy to implement in both the digital and analog domain. Because of this, there are seemingly limitless approaches that have been demonstrated to function well. However, with traditional approaches, there exists two areas that can still be improved on.

First, a fixed filter approach indicates that the passband is unchangeable. For applications in which frequency of interest may change over time, excess noise is captured outside the bandwidths of the region of signal power in this approach. For a simple case of a cognitive radio in which the center frequency of the signal changes across two fixed values, the excess noise of a fixed-filter approach can be visualized in Figure 1.2.1a. To tackle this, there have been many approaches to develop filters that can switch between specific passbands, such as [13]-[15]. These methods do an adequate job of filtering out the excess noise that would otherwise be captured by a traditional fixed-bandpass approach, as visualized in Figure 1.2.1b. One such method, "time-frequency peak filtering" [16]

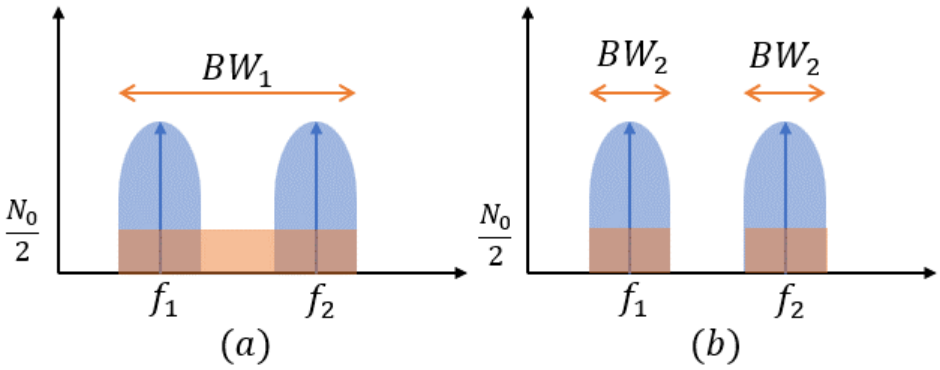

Figure 1.2.1: Comparison of filter noise bandwidths across fixed filters (a), and traditional tunable filter banks (b) across two discrete frequencies. The brown indicates the captured noise.

provides a correlation-based method to accomplish this. Another popular approach is the switched filter bank method [17]-[19], in which designated passbands filters are all constructed and utilized corresponding to which frequency is desired. For transmitted signals in which the carrier frequency is hopped between predetermined values, these approaches do an adequate job of filtering out the excess noise outside of the desired bandwidths at a given period of time.

The second area that can be improved upon is the settling time of each of these filters. If we choose to work with Frequency-Shift Keyed (FSK) signals in which the carrier frequency switches at rates corresponding to the symbol rate of the signal, traditional tunable filters would be inadequate to filter out the noise in-between the regions of signal power. This is because many of these filters fall short of switching at rates faster than the symbol rate of a signal and at times struggle with issues in maintaining charge, thus disqualifying them from being utilizable for FSK modulated signals in real time. With the foreknowledge of the signal phase/frequency shifts readily available, dynamic filtering can filter signals across varying frequencies/phases and even further minimize the noise to a bandwidth corresponding to that of the baud-rate of a given signal without the constraint of "resettling", despite what the Q of the filter may be.

1.3 The Infinite Impulse Response (IIR) Filter

In this thesis, much of the groundwork behind demonstrating the theory of dynamic filters builds on the theory of IIR filters, a type of recursive filter. Recursive filters are filters that are implemented in the time domain (in contrast to FFT filtering, which takes place in the frequency domain). Compared to traditional convolutional filtering, recursive filters provide an effective way of achieving a long impulse response without having to perform a long convolution. These long impulses are theoretically infinite, which is why another term for these types of filters are infinite impulse response filters (IIR). They usually take the following form:

$$y[n] = \sum_{i=0}^{A} a_n x[n-i] + \sum_{i=1}^{B} b_n y[n-i] \tag{1.3.1}$$

The coefficients in front of the values are often also called "taps", and they are what characterize the filters. In contrast to IIR filters, Finite Impulse Response (FIR) filters do not contain the secondary feedback term and lack an infinite response – as such, their filtering time constant is short, therefore they will not be considered for the purpose of this research. For the purposes of this work, only a single-pole complex IIR filter will be covered. Usually, single-pole IIR filters are only utilized for low-pass or high-pass filtering, but we observe that the usage of complex variables enables us to shift the pass-band frequency of a low-pass filter up to a specific frequency. The typical single-pole digital IIR filter takes the following form:

$$y[n] = ax[n] + by[n-1] \tag{1.3.2}$$

For single-pole IIR filters, the values of a and b are chosen based on the desired normalized cutoff frequency, and are traditionally held to observe the following relationship [8]:

$$b = e^{-2\pi f_{cutoff}} \tag{1.3.3}$$

$$a = 1 - b \tag{1.3.4}$$

$$f_{cutoff} = \frac{\ln(b)}{-2\pi} \tag{1.3.5}$$

Where f_{cutoff} is the normalized cutoff frequency of the lowpass filter. Although, Equation (1.3.3) is not a necessary condition for IIR filtering to take place, it serves as a fundamental condition in which other characteristics (such as the cutoff frequency) can be derived. Using the z-transform of the one-pole filter, the transfer function can be solved algebraically:

$$Y[z] = aX[z] + bY[z]z^{-1} \tag{1.3.6}$$

$$H[z] = \frac{Y[z]}{X[z]} = \frac{a}{1 - bz^{-1}} \tag{1.3.7}$$

1.4 Thesis Outline

In this thesis, a theoretical model for dynamic filtering is proposed, as well as an approach towards physical realization of such a filter. The mathematical baseline for the filtering procedure is introduced in Chapter 2. The theory of time-varying transmission lines (TVTL) and how they can be repurposed as dynamic filters is highlighted in Chapter 3. Subsequently, Chapter 4 proposes an application in the front-ends of traditional transceiver systems. Finally, Chapter 5 concludes this thesis and foregrounds future progress in this work and additional research directions.

CHAPTER 2

Phase-Sensitive Dynamic Filtering

In this chapter, the traditional recursive IIR filter theory is covered with the addition of applying dynamically switched coefficients in order to demonstrate the theory of dynamic filtering. This is done to highlight the frequency and phase shifting features of utilizing complex variables with IIR filters. The theoretical performance of such a filtering procedure with regards to noise level is also analyzed. Next, a theoretical simulation setup can be constructed to demonstrate the behavior of the equivalent dynamic filter across two different types of commonly used signal schemes (BFSK and QPSK) to demonstrate the frequency and phase sensitivity of such a filter.

2.1 Complex IIR Filtering – Frequency Selectivity

As shown by Crystal and Ehrman [1], by substituting in $z_{shift} = e^{-j\omega_c T} z$ into Equation (1.3.6) we can effectively shift the passband of the frequency from 0 to ω_c. This produces the following equation:

$$H_{complex}[z] = \frac{a}{1 - be^{j\omega_c T} z^{-1}} = \frac{a}{1 - b' z^{-1}} \tag{2.1.1}$$

$$b' = be^{j\omega_c T} = be^{j2\pi\left(\frac{f_c}{f_s}\right)} \tag{2.1.2}$$

Where b' is a complex coefficient, and $T = 1/f_s$ is the sampling interval. It is worth noting that this procedure is essentially the modification of the feedback term in the recurrence relation. Using the inverse z-transform, the impulse response of the complex IIR filter can also be solved to be:

$$h[n] = a \cdot b'^{n} u[n] \tag{2.1.3}$$

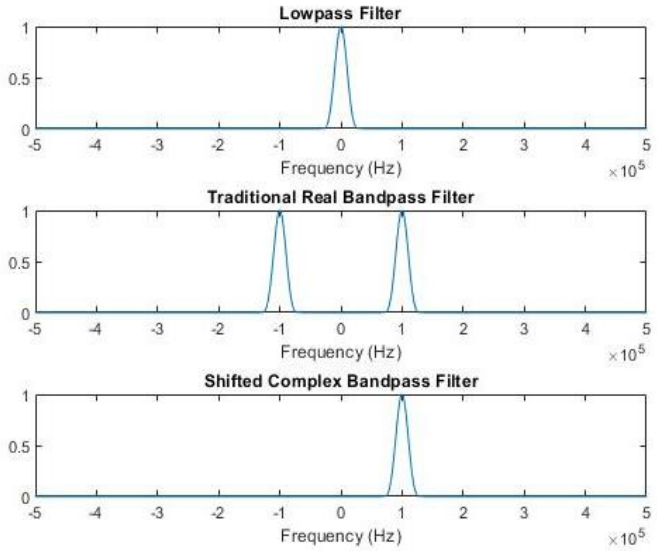

Figure 2.1.1: Comparison of frequency responses across lowpass filters, traditional bandpass filters, and complex IIR filters.

Such filters are non-symmetric about the zero-frequency axis (something characteristic of purely real filters) in the frequency domain. The center point of the filter is shifted according to the ω_c value that is selected. When starting with a real low-pass IIR filter, the symmetry of the entire frequency response characteristic about the center frequency is preserved. The final response is identical to the positive frequency axis of a traditional bandpass filter that is transformed from the corresponding low-pass prototype. Because of this, the original cutoff frequency of the lowpass filter becomes half the bandwidth of the shifted complex bandpass filter. This can be seen in Figure 2.1.1. Furthermore, as can be observed by Equations (1.3.2) and (1.3.7), this method of filtering can be performed either in the time domain (via recursive filtering) or in the frequency domain (via FFT filtering). However, in dynamic filtering, only the time domain recursive filtering will be explored. In this form of filtering, it is also worth noting that the lowpass to bandpass transformation, which is traditionally utilized for transformations towards the digital domain, is not utilized. The reason for this is that we desire to keep the exponential in its complex form, rather than using the typical transformation to

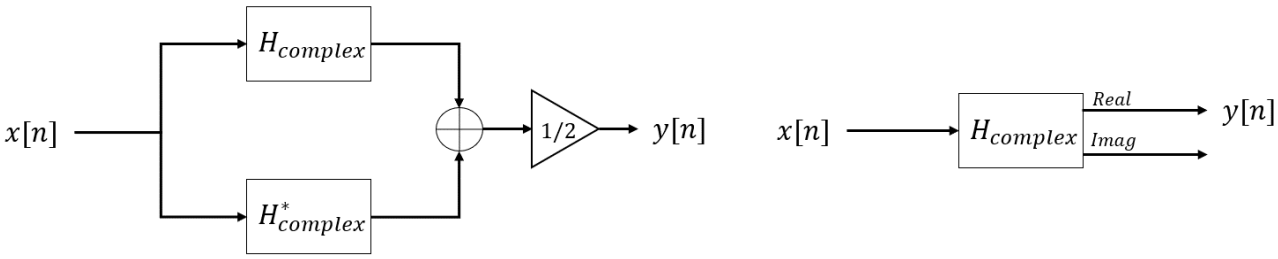

Figure 2.1.2: Comparison of two equivalent ways of obtaining the output of a complex filter

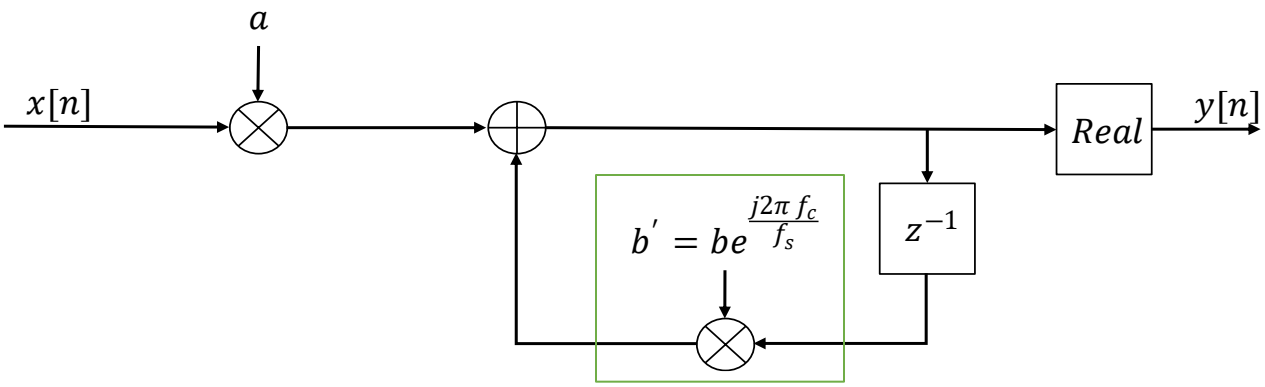

Figure 2.1.3: Representation of first-order frequency-tunable complex IIR filter.

make it purely real. Additionally, performing this transformation doubles the number of coefficients, making it an unsuitable condition for dynamically switching the passband in real time.

Finally, as demonstrated by Regalia and Mitra [3], only the real portion of the output is considered. For this example, since the real equivalent of $H_{complex}$ is characterized by the sum of $H_{complex}$ and its complex conjugate, $H^*_{complex}$, the real portion of the output from $H_{complex}$ matches the desired output, $y[n]$, from that of the real equivalent. The imaginary component can be neglected for the final output, indicating that only a single complex filter is adequate to compute the output of the equivalent real filter. This operation can be visualized in Figure 2.1.2, and the first order representation of such a filter can be seen in Figure 2.1.3. From this, we have demonstrated a way to model the frequency-selectivity of dynamic filters in the form of IIR filters with a complex feedback coefficient.

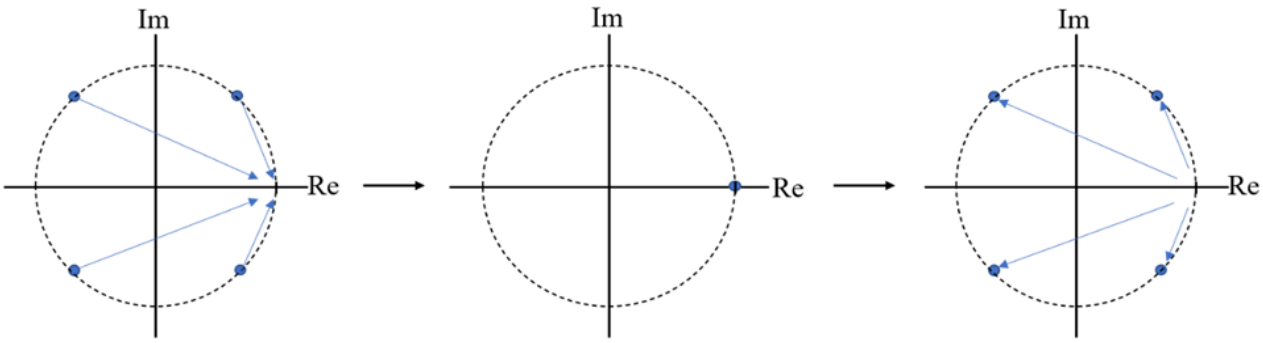

Figure 2.2.1: Effects of nullifying and reconstructing phase for a QPSK constellation

2.2 Complex IIR Filtering – Phase Adjustability

Phase-modulated signals make up a large part of virtually any current operational communications system. However, they run into issues with narrow pass-band filters – namely, distortion [10]. This is because a signal through such a channel results in the removal of key frequency components in the transitions between phases. As a result, to preserve the sharp phase shifts of a phase-shift-keyed (PSK) signal, the passband of the filter must be increased to sizes larger than desired. Applying pulse-shaping to remedy this also increases the bandwidth to a value typically twice that of the symbol rate. Because of this, more of the spectra is admitted into the receiving system, resulting in more noise, and undesired frequencies. In the same way that the center pass-band frequency for complex IIR filters can be switched, we will now proceed to show that the phase of the signal can also be dynamically followed through this dynamic filtering procedure. The first part involves "nullifying" the phase of the input signal through the feedforward term. This is more clearly visualized in the time domain:

$$y[n] = a'x[n] + by[n-1] \tag{2.2.1}$$

$$a' = e^{j\phi}a \tag{2.2.2}$$

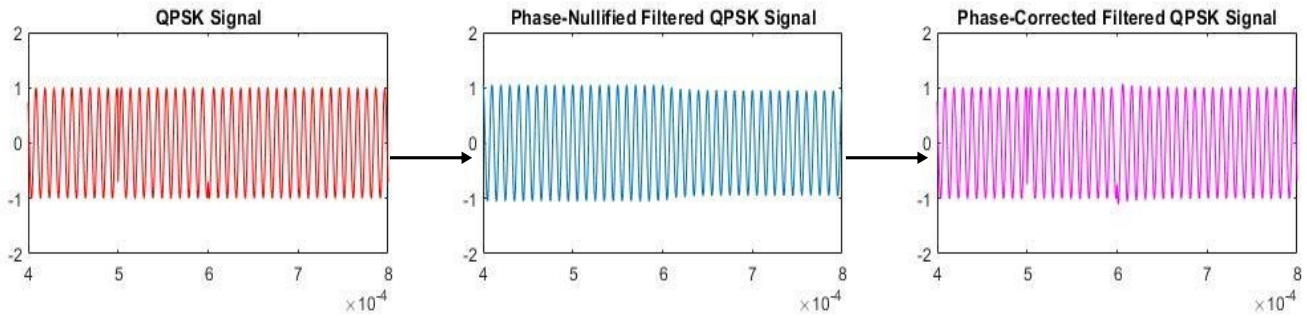

Figure 2.2.2: Phase-sensitive filtering process in the time domain

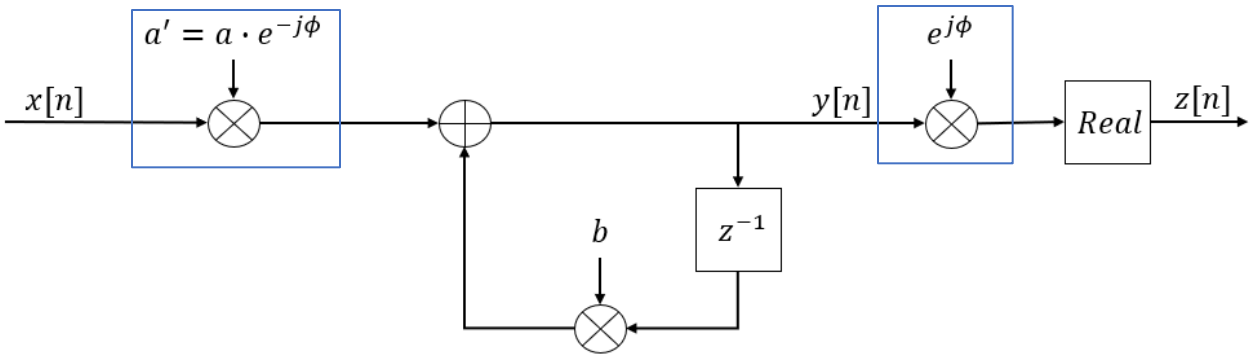

Figure 2.2.3: Representation of first-order phase-adjustable complex IIR filter.

Where ϕ is the temporal instance of the phase of the incoming signal, and a' is the complex coefficient corresponding to the desired phase shift. It can be observed from Equation (2.2.1) that in contrast to the frequency selective procedure from the previous part, the complex coefficient is in the feed-forward term rather than the feedback term.

As can be seen in Figure 2.2.1, the constellation of a traditional QPSK signal is plotted. The arrows indicate the rotation affects that the phase shift, ϕ, have on the constellation of the filtered waveform, mapping completely to the positive real domain. As can be observed in Figure 2.2.2, the time-domain of the phase-corrected QPSK signal is compressed to simply a sinusoid, as all the different phases have been matched to one shared phase, thus reducing the bandwidth. The final portion of part of this filtering process involves re-correcting (or reconstructing) the phase. This can be simply done by adding the same exponential multiplier (with inverted phase) to the output of this filtering process. Once more, only the real component is considered. The relation is as follows:

$$z[n] = Re\{e^{-j\phi}y[n]\} \tag{12}$$

The phase-sensitive filtering procedure can be visualized in Figure 2.2.3.

2.3 System-Level Overview

The full dynamic filtering procedure can be visualized in Figure 2.3.1. In digital communications, dynamic filters are recursive filters that are implemented in the time domain. These recursive filters become "dynamic" through the changing of the coefficients which dictate the bandwidth of the filter passband. For the complex filters that have been covered, these coefficients are complex. The phase of the coefficients determines the center frequency of the overall response (or passband frequency) and enacts a "nullification" and "reconstruction" effect on the overall phase of the signal. The amplitude of the coefficients determines the bandwidth of the overall response. Implementing digital filters such as these are straightforward in the digital domain. One must swap the coefficients of the filter in accordance with the desired switching requirements, and this can be done in real time. The number of sets of coefficients depends on the number of unique passbands and/or phase shifts that are desired:

$$y[n] = \sum_{i=0}^{A} a_n' x[n-i] + \sum_{i=1}^{B} b_n' y[n-i] \qquad n \in \{1,2,\dots\} \tag{2.3.1}$$

Where a_n' and $b_n{}'$ are the complex coefficients. Regarding the current single-pole complex IIR filter being explored, the recurrence equation will take the following form:

$$y[n] = a_i x'[n] + b_i' y[n-1] \tag{2.3.2}$$

$$z[n] = Re\{e^{-j\phi}y[n]\} \tag{2.3.3}$$

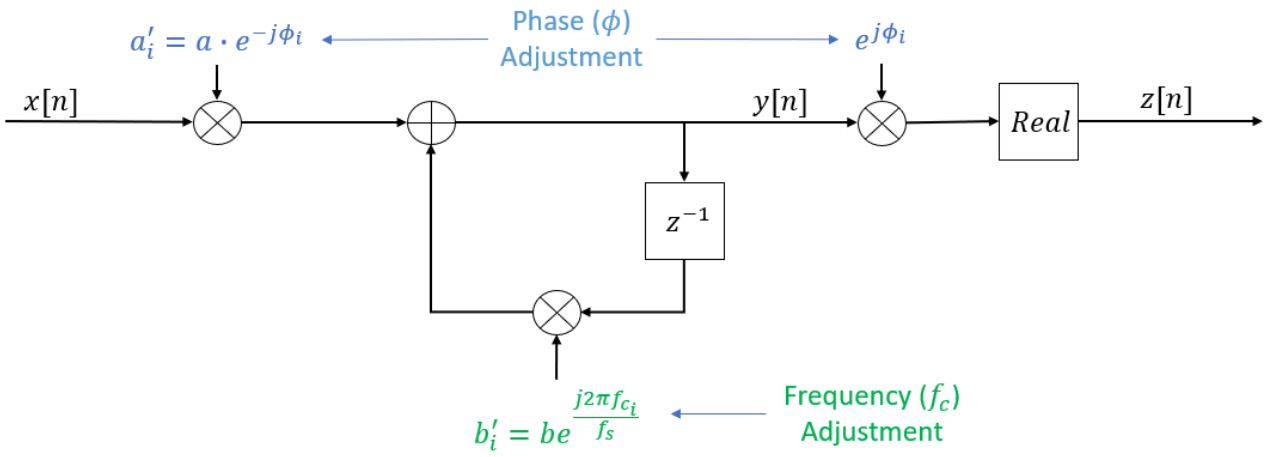

Figure 2.3.1: Full Dynamic Filter Setup

Evidently, as these complex coefficients are changed, the passband is also changed corresponding to the pair of chosen coefficients. The key here for dynamic filtering is that the "charge" is conserved across frequency shifts. In other words, the filter does not need to "resettle" to a new passband, which is something characteristic of traditional tunable bandpass filters. This is due to the fact that settling time (or charging time) is dependent on the time constant of the filter, which is then dependent on the magnitude of the coefficients, not the phase. This implies that merely changing the phase of the coefficients not only does not influence the time constant, but also removes the settling effect imposed by the time constant. Or more mathematically put, for IIR filters it follows that [9]:

$$|b| = e^{-\frac{1}{d}} \tag{2.3.4}$$

Where d is the time constant of the single-pole complex filter. This is important for real-time switching configurations, as the settling time is directly correlated to the selected bandwidth of the complex IIR filter. The time constant must be much greater than the symbol period to preserve the energy between shifts, which is stored in both the real and complex parts of the signal. Consequently, the narrower the desired bandwidth, the longer it takes for the system to settle to steady state. For standard communications systems in which the bandwidth occupies less than 5 percent of the carrier

frequency, this settling time may take hundreds to thousands of bits, which makes traditional filter switching inadequate for real-time symbol-level switching. Therefore, the preservation of charge in dynamic switching introduces a clean way to switch between passbands, which would be especially desired in frequency-modulated signals.

In a typical communications system, noise should always be considered. Traditionally, for a fixed-bandwidth approach to designing a bandpass filter such as that depicted in Figure 1.1.2a, the captured noise power that remains unfiltered out is as follows:

$$P_{N1} = \frac{B_{N1} \cdot N_0}{2} = \left((f_1 - f_2) + \Delta f_{eff}\right) \cdot \frac{N_0}{2} \tag{2.3.5}$$

Where Δf_{eff} is the effective bandwidth corresponding to the effective symbol rate (which is dependent on the shape of the pulse). For traditional switched filters with passbands that follow the respective frequency of propagation, the noise power is as follows:

$$P_{N2} = \Delta f_{eff} \cdot \frac{N_0}{2} \tag{2.3.6}$$

As can be observed, the captured noise power is less, and does not include the frequency-range across the two carriers from which the signal hops. Finally, for the dynamic filtering approach, assuming precursor knowledge of the frequency or phase modulated signal is held, the amount of noise power follows the expression:

$$P_{N3} = \Delta f_{dyn} \cdot \frac{N_0}{2} = \frac{\ln|b'|}{-\pi} \cdot \frac{N_0}{2} \tag{2.3.7}$$

Where Δf_{dyn} is the bandwidth of the dynamic passband and can be derived from Equation (1.2.5), and b' is the complex feedback coefficient in the integration process as seen in Figure 2.3.1. As mentioned before, the narrower the bandwidth, the longer the time constant of the filter – which is

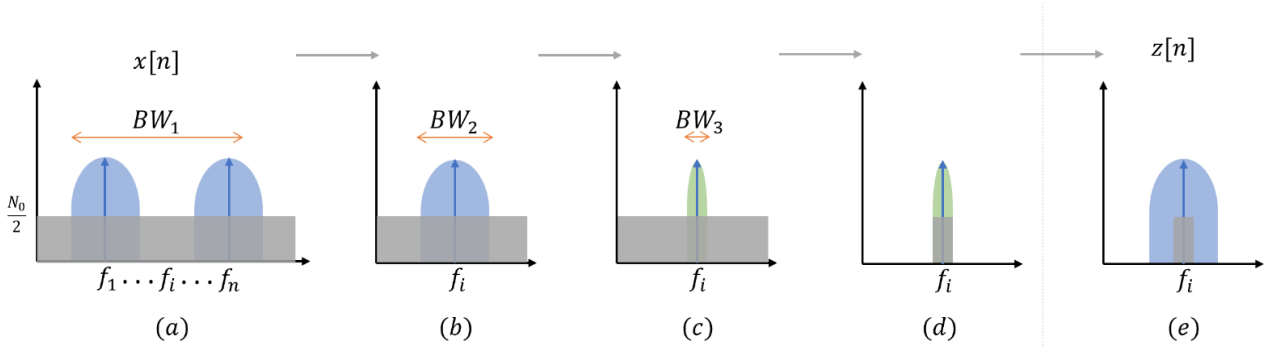

Figure 2.3.2: Progression of noise suppression in dynamic filtering process from a systems perspective.

(a) Signal spectrum with multiple center frequencies. (b) Narrowing in a single frequency. (c) Signal phase is nullified to decrease the bandwidth. (d) Excess noise is filtered out. (e) Phase is recorrected, thus resulting in less noise captured.

desired. Additionally, after the phase correction, the bandwidth of the signal becomes compressed, and the passband only needs to be selected such that it sufficiently captures the sinusoids of the varying frequencies. Thus, the bandwidth corresponding to how much noise is carried through the filtering process can ideally be limited directly down to a fraction of the value, only passing through noise which perfectly correlates with the desired signal. After correcting the phase, the resulting noise is at least less than that of the traditional switched bandpass filters. This noise-filtering process can be visualized in Figure 2.3.2.

2.4 Modulated Waveform Simulations

For a BFSK signal, using a fixed bandpass filter on such a signal will attenuate one of the transmitting frequencies over the other, even though both are equally necessary components of the signals. Simply put, when the received frequency is within the passband frequency, the output values seem to "charge" towards a certain limit. When the frequency shifts to one that is outside the passband, the output "decays" towards 0. This is a characteristic of the recursive nature of filters. Additionally, if one attempts to utilize a traditional tunable filter with switched filter banks to filter a BFSK signal in real-time, there will be a settling-time for each symbol transition, leading to an unclean filtering output. To combat this, we apply the dynamic filtering method. As mentioned before, we individually utilize

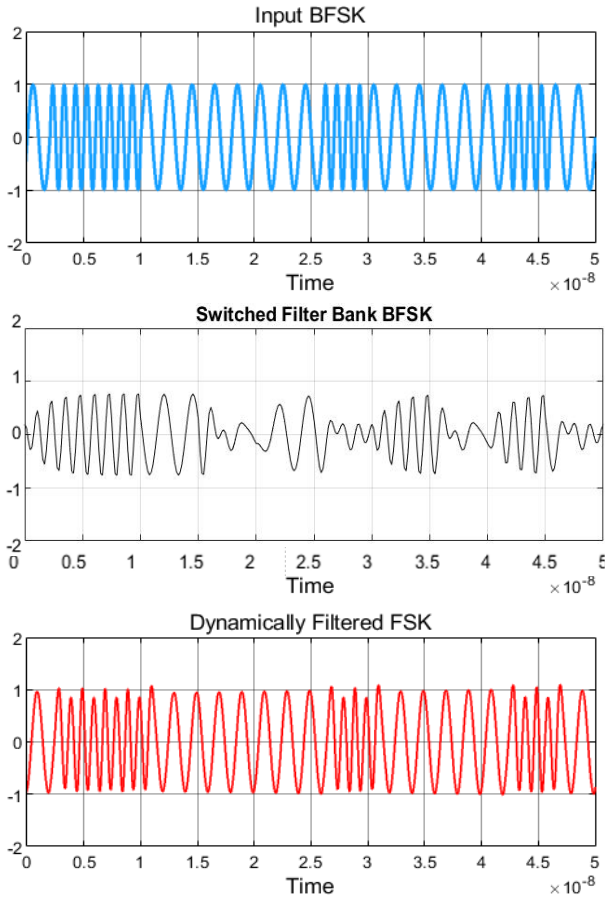

Figure 2.4.1: Comparison between switched-bandpass methods, and dynamically filtered methods utilizing the same bandwidth across BFSK signals.

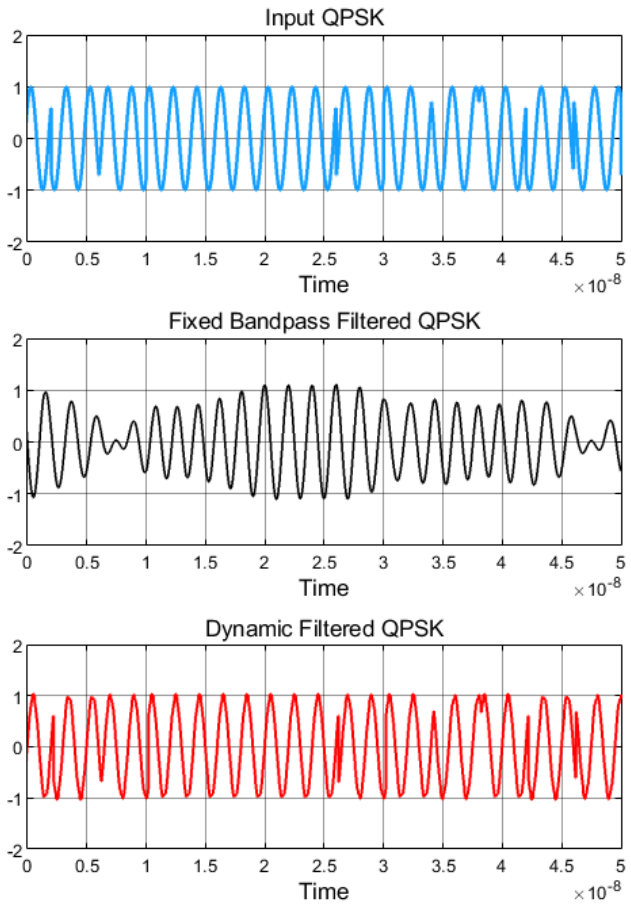

Figure 2.4.2: Comparison between switched-bandpass methods, and dynamically filtered methods utilizing the same bandwidth across QPSK signals.

each pair of coefficients of the two passband frequencies at instances in time in which their corresponding carrier frequencies are present. For example, when bit '0' is being transmitted, f_1 is the carrier frequency; therefore, we will apply the pump signal with a passband frequency corresponding to f_1. When it switches to bit '1' being transmitted, we switch the filter to the other passband frequency. To do this, we must know the exact instances in time when the frequency switches. The simulation setup is performed on MATLAB. As can be observed in Figure 2.4.1, the "charge" for the filtered signals is preserved between frequencies shifts. Essentially, there is no discharging affect between frequency switches, as explained in the previous section.

For the QPSK-modulated signal, the phase is no longer continuous across the entire duration. As such, rather than modifying the frequency of the pump signal, the phase of the feedforward coefficient, a', must be switched corresponding to the phase shifts in the transmitted QPSK signal. As seen before, this means that knowledge of the time-domain bit stream is a prerequisite to properly utilizing the TVTL as a dynamic filter. There is a preservation of waveform with this filtering method. As can be observed in Figure (2.4.2), the precise phase-changes are lost in the filtering process for a fixed bandpass filter with narrow bandwidth but are preserved for the dynamic filtering method. From this theory, it is clear that filters such as these can be quite useful; however, the theory in itself is not sufficient in itself to be beneficial in any way. In the next chapter, we will explore a potential candidate for physically realizing dynamic filters.

CHAPTER 3

Time-Varying Transmission Line (TVTL) Filter

In this chapter, the theory of the time-varying transmission line is explored in order to detail why it can be a suitable candidate for dynamic filtering. First, the focus will be on the theory behind how the TVTL produces parametric amplification to incoming signals. After this, we explain how two TVTLs can be cascaded such that they begin to exhibit filtering characteristics and we derive time-domain functions resembling that of the dynamic filter. Finally, simulation results indicating the adequacy of the TVTL as a dynamic filter are presented.

3.1 Theory of the Time-Varying Transmission Line (TVTL)

The time-varying transmission line is a transmission line with directional parametric conversion effects. The theory behind the TVTL was first explored in [26]-[27] in the late 1950's utilizing time-varying inductance, being called a "Traveling-Wave Parametric Amplifier". The work has since been revisited [25] with a more physical and discrete realization, then called "Distributedly Modulated Capacitors". Finally, it was not until recently [21] that it would now be called the TVTL, which is what we will identify it as in this work. Recent studies in the TVTL were initially organized with the intention of studying its non-reciprocal affects and non-magnetic properties. Over time, the use of the TVTL began to expand towards other communications front-end applications such as mixers [23], amplifiers [24], and correlators [28] due to its unique amplification and directional affects. Before beginning to demonstrate that the TVTL can be utilized as a filter, it is first helpful to understand the concepts upon which it is grounded on.

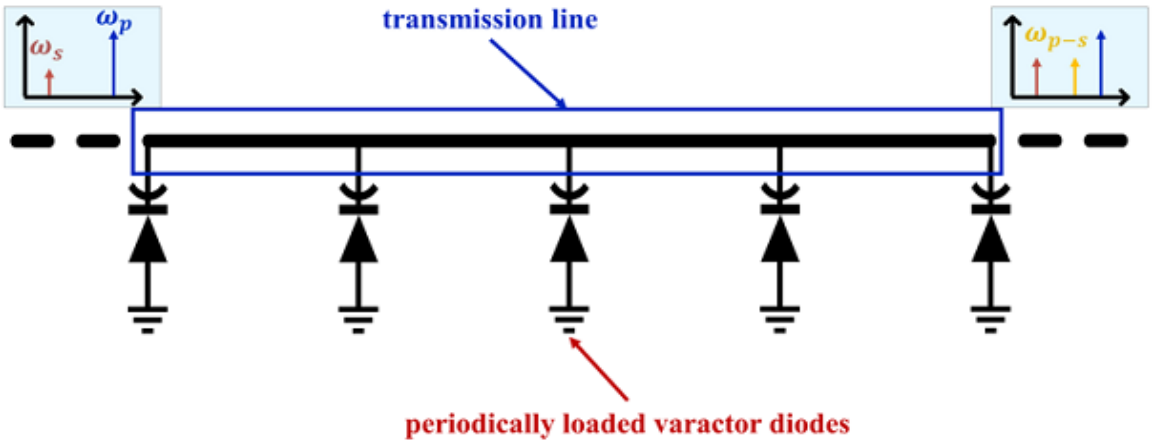

Figure 3.1.1: Diagram of TVTL with periodically loaded varactor diodes. An input signal at frequency ω_s along with a pump at frequency ω_p generates a frequency at ω_{p-s} [24]

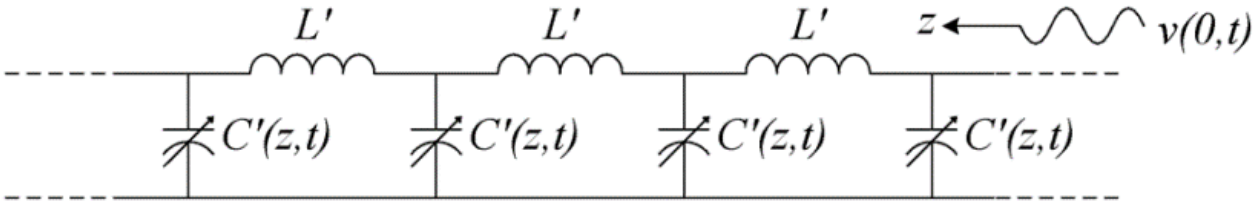

Figure 3.1.2: Lumped-element model of the TVTL [29]

Figure 3.1.1 illustrates the physical structure of the TVTL. Functionally, we can observe that an input signal at the frequency ω_s is sent through the TVTL, causing modulated frequencies along the pump frequency to be generated at ω_{p-s} and ω_{p+s}. The upper frequency is ideally pushed outside of the cutoff frequency as seen in Figure (3.1.1). Effectively, the TVTL circuit has both passive and active components – both of which are fundamentally low loss and low noise. As observed in the figure, the TVTL can be constructed with discrete varactor diodes periodically in shunt with a traditional passive transmission line [24]. In doing this, we are able to modulate the voltage of an electromagnetic wave, also known as the pump wave – hence the "time-varying" aspect in its name. A lumped-element model of the TVTL can be seen in the following Figure 3.1.2. Using this model, we will be showcasing prior work in deriving the input/output voltage

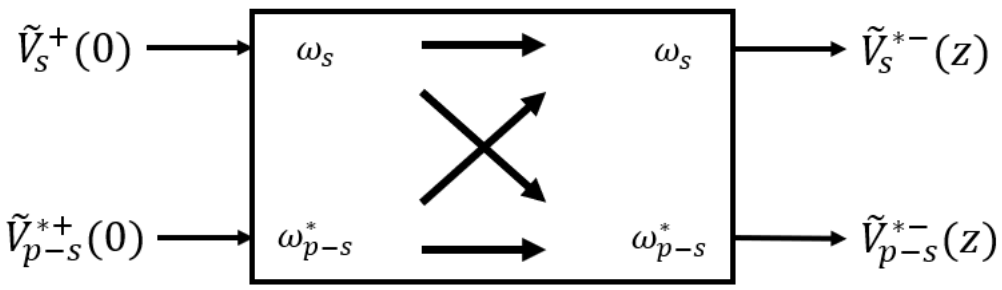

Figure 3.1.3: System-level diagram of the TVTL – taking the form of a four-port linear network.

equations which will be utilized in this study. Starting from telegrapher's equations (3.1.1 - 3.1.2), we can set the conditions from which the relations for the model above can be produced [22]:

$$\frac{\partial v(z,t)}{\partial z} = -L'\left(\frac{\partial i(z,t)}{dt}\right) \tag{3.1.1}$$

$$\frac{\partial i(z,t)}{dt} = -\frac{\partial\big(C'(z,t)v(z,t)\big)}{\partial t} \tag{3.1.2}$$

Using Equations (3.1.1) and (3.1.2), we can derive the following wave equation for the lumped-element TVTL model:

$$\frac{\partial^2 v(z,t)}{\partial z^2} = L\frac{\partial}{\partial t}\left[C(z,t)\frac{\partial v(z,t)}{\partial t}\right] \tag{3.1.3}$$

Assume the following condition that the TVTL is non-dispersive:

$$v_p = \frac{\omega_s}{\beta_s} = \frac{\omega_{p-s}}{\beta_{p-s}} = \frac{\omega_p}{\beta_p} = \frac{1}{\sqrt{LC_0}} \tag{3.1.4}$$

Where v_p is the phase-velocity of the traveling wave, and β_i is the propagation constant at the i'th frequency of interest. These equations and assumptions used to set the foundation for all

derivations involving the TVTL. Assuming that output frequencies are confined to only include the frequency of the original signal and the idler signal (ω_{p-s}), we can view the TVTL from a more system-level approach using the 4-port linear diagram seen in Figure 3.1.3. Relations have already been derived between the input/output voltages in the form of a matrix equation as a function of space and frequency [24]:

$$\begin{bmatrix} \tilde{V}_s^-(z) \\ \tilde{V}_{p-s}^{*-}(z) \end{bmatrix} = \begin{bmatrix} t_{11} & t_{12} \\ t_{21} & t_{22} \end{bmatrix} \begin{bmatrix} \tilde{V}_s^+(0) \\ \tilde{V}_{p-s}^{*+}(0) \end{bmatrix} \tag{3.1.4}$$

Where:

$$\begin{bmatrix} t_{11} & t_{12} \\ t_{21} & t_{22} \end{bmatrix} = \begin{bmatrix} a_{11}e^{-(\alpha_s + j\beta_s)z} & a_{12}e^{(-\alpha_s + j\beta_s)z} \\ a_{21}e^{-(\alpha_{p-s} - j\beta_{p-s})z} & a_{22}e^{-(\alpha_{p-s} - j\beta_{p-s})z} \end{bmatrix} \tag{3.1.5}$$

Where:

$$\begin{bmatrix} a_{11} & a_{12} \\ a_{21} & a_{22} \end{bmatrix} = \begin{bmatrix} \cosh(\lambda\, z) & -je^{j\phi_p}\sqrt{\dfrac{\beta_s}{\beta_{p-s}}}\sinh(\lambda\, z) \\ -je^{j\phi_p}\sqrt{\dfrac{\beta_{p-s}}{\beta_s}}\sinh(\lambda\, z) & \cosh(\lambda\, z) \end{bmatrix} \tag{3.1.6}$$

Where $\lambda = \frac{\xi_0\sqrt{\beta_s\beta_{p-s}}}{4}$, α_i is the propagation attenuation constant of the TVTL at frequency 'i', and ξ_0 is the capacitance modulation index of the TVTL. With this, we can now proceed to the derivation of transfer function and time-varying recurrence relation of the TVTL:

3.2 TVTL Filter Derivation

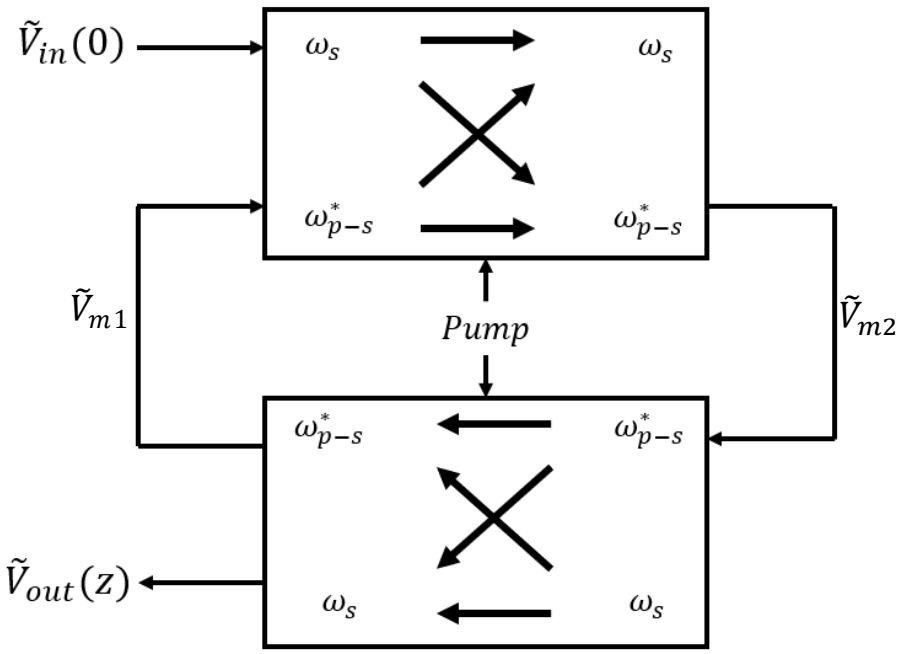

Figure 3.2.1: System-level diagram of the TVTL Filter – cascading the output of one to the input of the other.

The most recent TVTL work consists of creating a feedback loop by feeding back the output of the idler path to the input [24]. In this study, we are interested in cascading the TVTL in the manner depicted in Figure 3.2.1. From the voltage relationships derived in Equations (3.1.4) – (3.1.6), and assuming that there is no propagation delay between the two TVTL's, we can start with the following equations as a basis:

$$\tilde{V}_{out} = \tilde{V}_{m2} t_{12} \tag{3.2.1}$$

$$\tilde{V}_{m1} = \tilde{V}_{m2} t_{22} \tag{3.2.2}$$

$$\tilde{V}_{m2} = \tilde{V}_{in} t_{21} + \tilde{V}_{m1} t_{22} \tag{3.2.3}$$

From reorganization Equations (3.2.1) - (3.2.3), we can derive the following transfer function for the input/output voltage at the signal frequency:

$$\tilde{V}_{out} = \left(\frac{t_{12}t_{21}}{1 - t_{22}^2}\right) \cdot \tilde{V}_{in} \tag{3.2.4}$$

Using the values of t_{ij} from Equation (3.1.5), we can substitute the values of t into this transfer function:

$$\tilde{V}_{out} = \left(\frac{a_{12}a_{21}e^{-j2\beta_s z}}{1 - a_{22}^2 e^{j2\beta_{p-s} z}}\right) \cdot \tilde{V}_{in} \tag{3.2.5}$$

From the coefficient definitions from Equation (3.1.6), we are left with the following expanded transfer function:

$$\tilde{V}_{out} = \frac{\sinh^2(\lambda z)\, e^{-(\alpha_s + \alpha_{p-s})} e^{j\beta_p} e^{j2\beta_s z}}{1 - \cosh^2(\lambda z)\, e^{-2\alpha_{p-s} z} e^{-j2\beta_{p-s} z}} \cdot \tilde{V}_{in} \tag{3.2.6}$$

From this equation, the first thing we observe is that there is a resonance condition for this filter. In Equation (3.2.5), we first assume that the coefficient of a_{22}^2 takes a value with magnitude less than 1 in order to keep the system stable. In order to achieve maximum voltage amplification, we can distinguish the following condition:

$$2\beta_{p-s} z = 2n\pi \tag{3.2.7}$$

Where *z* is the length of the TVTL, and *n* is a non-negative integer. Assuming a non-dispersive behavior, simplifying this results in:

$$(\omega_p - \omega_s)\tau = n\pi \tag{3.2.8}$$

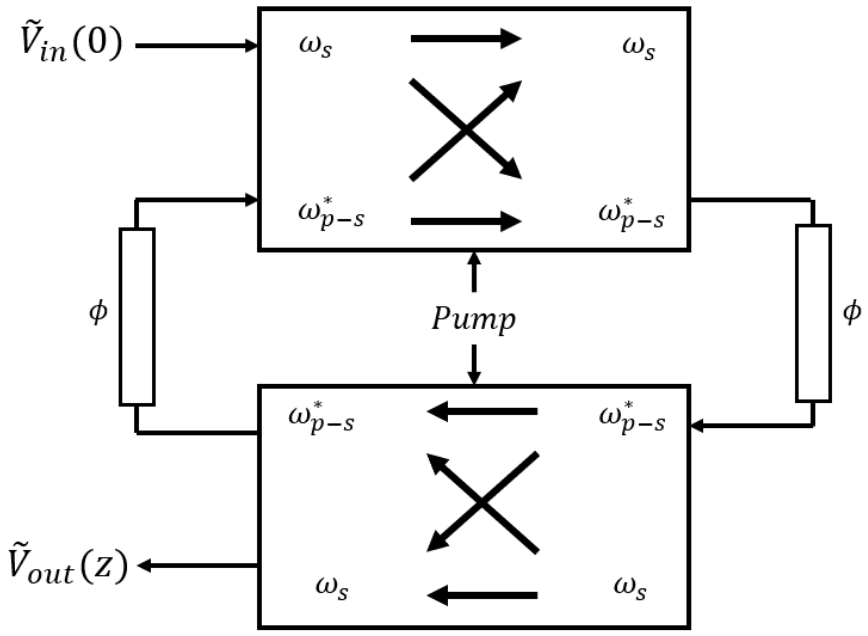

Figure 3.2.2: System-level diagram of the TVTL Filter with added delays

Where τ is the time it takes for a wave to propagate through the system. With this condition set, we can find the condition for resonance:

$$f_{p-s} = \frac{n}{2\tau} \tag{3.2.9}$$

From this equation, we can observe that a resonance can be formed at the converted frequency if the length of the TVTL is chosen such that the propagation time, τ, meets the criteria in Equation (3.2.9). However, if the length of the TVTL is not a variable that can be easily changed, the resonance can also be tuned by fixing a delay between the two TVTL's, as seen in Figure 3.2.2. They are chosen to fulfill the updated resonant equation:

$$f_{p-s} = \frac{n}{2\tau} - \frac{\phi}{2\pi\tau} \tag{3.2.10}$$

It is important to realize here in this equation that the idler frequency, f_{p-s}, is fixed. Meaning that After fixing the delay lengths of the TVTL and added delays, we can effectively change the center passband frequency, f_s, by changing the pump frequency, f_p:

$$f_s = f_p - f_i = f_p - f_{p-s} \tag{3.2.11}$$

This produces a wide tuning range, since throughout the tuning process, the resonant idler frequency is not altered. Meaning that even when the pump frequency is used to change the passband of the filter, we expect the resonant idler frequency in the loop to stay consistent throughout that switch. From Equation (3.1.6), we also observe that the phase of the upconverted idler frequency can also be modulated to that of the pump signal.

Essentially, this procedure starts by first upconverting the input frequency to a high-Q sinusoidal tone at the idler frequency (ω_{p-s}) with the initial TVTL, and then finally downconverting the signal back to the original frequency (ω_s). Since the TVTL is typically equipped with diplexers at the input and output (intended to separate out the idler frequency), ideally all other frequencies other than the idler frequency are attenuated by the time we reach the output of the TVTL Filter. The resonant condition of this filter results in an energy-conversion process in both stages: 1) The energy of the pump frequency to produce the idler frequency, and 2) The idler frequency to be coupled back to the energy of the signal frequency and to create amplification. Additionally, we can see from Equation (3.2.6) that as the pump power increases, the modulation capacitance index, ξ_0, also increases. This brings the value of the t_{22} coefficient closer to one, significantly increasing that gain, frequency-selectivity, and Q of the overall filter.

In summary, from this we can draw three conclusions. The TVTL offers:

1. Suppression in frequencies outside of the signal frequency.

2. Amplification in the signal frequency due to the parametric coupling effect of the added pump frequency and the idler feedback resonance condition.

3. Tunability of the passband frequency by directly altering the pump frequency with a wide tuning range, since the resonance frequency is not altered.

4. Direct phase-modulation of the upconverted idler frequency by modulating the phase of the pump signal. Conversely, the phase of the downconverted signal frequency can be modulated directly in the same way.

With this, we are interested in deriving the time-domain recursive relations for this approach to obtain the theoretical performance for this filter for dynamic filtering. The first step is to rewrite the propagation constant to one that utilizes more familiar units for Fourier analysis:

$$\beta_{p-s}z = \frac{\omega_p}{v_p}z - \frac{\omega_s}{v_s}z = \omega_p\tau_p - \omega_s\tau_s \tag{3.2.12}$$

With this, we can translate the same initial frequency-space equations used previously (3.2.1) - (3.2.3) into the time-domain with respect to ω_s:

1. $$\begin{aligned} F^{-1}\{\tilde{V}_{out}\} &= a_{12}\cdot F^{-1}\{e^{-j\omega_s\tau_s}\cdot\tilde{V}_{m2}^*\} \\ &= a_{12}\cdot\frac{1}{2\pi}\int\left(e^{-j\omega_s\tau_s}\cdot\tilde{V}_{m2}^*\right)\cdot e^{j\omega_s t}d\omega_s \\ &= a_{12}\cdot\left(\frac{1}{2\pi}\int\left(\tilde{V}_{m2}\cdot e^{j\omega_s(\tau_s-t)}\right)d\omega_s\right)^* \\ V_{out}(t) &= a_{12}\cdot V_{m2}^*(\tau_s - t) \end{aligned} \tag{3.2.13}$$

2. $F^{-1}\{\tilde{V}_{m1}^*\} = a_{22} \cdot F^{-1}\{e^{j\omega_p\tau_p}e^{-j\omega_s\tau_s} \cdot \tilde{V}_{m2}^*\}$

$$= a_{22}e^{j\omega_p\tau_p} \cdot \frac{1}{2\pi}\int \left(e^{-j\omega_s\tau_s} \cdot \tilde{V}_{m2}^*\right) \cdot e^{j\omega_s t}d\omega_s$$

$$= a_{22}e^{j\omega_p\tau_p} \cdot \left(\frac{1}{2\pi}\int \left(\tilde{V}_{m2} \cdot e^{j\omega_s(\tau_s - t)}\right)d\omega_s\right)^*$$

$$V_{m1}^*(-t) = a_{22}e^{j\omega_p\tau_p} \cdot V_{m2}^*(\tau_s - t) \tag{3.2.14}$$

3. $F^{-1}\{\tilde{V}_{m2}^*\} = a_{21} \cdot F^{-1}\left\{e^{j\omega_p\tau_p}e^{-j\omega_s\tau_s} \cdot \tilde{V}_{m2}^*\right\} + a_{22} \cdot F^{-1}\{e^{j\omega_p\tau_p}e^{-j\omega_s\tau_s} \cdot \tilde{V}_{m1}^*\}$

$$= a_{21}e^{j\omega_p\tau_p} \cdot \frac{1}{2\pi}\int \left(e^{-j\omega_s\tau_s} \cdot \tilde{V}_{in}\right) \cdot e^{j\omega_s t}d\omega_s \ldots$$

$$\ldots + \ a_{22}e^{j\omega_p\tau_p} \cdot \frac{1}{2\pi}\int \left(e^{-j\omega_s\tau_s} \cdot \tilde{V}_{m1}^*\right) \cdot e^{j\omega_s t}d\omega_s$$

$$V_{m2}^*(-t) = a_{21}e^{j\omega_p\tau_p} \cdot V_{in}(t - \tau_s) + a_{22}e^{j\omega_p\tau_p} \cdot V_{m1}^*(\tau_s - t) \tag{3.2.15}$$

From reorganization Equations (3.2.12) - (3.2.15), we can derive the following time recurrence relation for the TVTL filter. If we set $y = V_{out}$ and $x = V_{in}$:

$$y(t) = a_{12}a_{21}e^{j\omega_p\tau_p} \cdot x(t - 2\tau_s) + a_{22}^2e^{j2\omega_p\tau_p} \cdot y(t - 2\tau_s) \tag{3.2.16}$$

Setting $a = \cosh^2(\lambda z)$ and $b = \sinh^2(\lambda z)$ and referencing the coefficient definitions from Equation (3.1.6), we can obtain the final recurrence relation:

$$y(t) = b \cdot e^{-(\alpha_{p-s}+\alpha_s)z}e^{j\omega_p\tau_p} \cdot x(t - 2\tau_s) + a \cdot e^{-2(\alpha_{p-s}z)}e^{j2\omega_p\tau_p}y(t - 2\tau_s) \tag{3.2.17}$$

Some further assumptions for the simplification of the theoretical relation are also made. First, we are assuming no dispersion, meaning that the propagation delays are the same (i.e., $\tau_s = \tau_p = \tau$). Next, we are assuming that this is a lossless system (i.e., $\alpha_s = \alpha_{p-s} = 0$). With this, we can simplify the final relation to the following equation:

$$y(t) = b \cdot e^{j\omega_p\tau} \cdot x(t - 2\tau) + a \cdot e^{j2\omega_p\tau}y(t - 2\tau) \tag{3.2.18}$$

With this relation, we can now proceed to the TVTL filter synthesis and simulations.

3.3 TVTL Filter Synthesis and Simulation

Simulations of this filter's performance are performed on Keysight's Advanced Design System. The first step in this simulation was to choose a suitable varactor diode model, as that makes up a fundamental portion of this parametric filtering technique. After that, the pumping structure for the diode used to mimic the traveling-wave behavior of the transmission line was formulated. Finally, the passive transmission-line structure is chosen. The measurements of the MMIC diode, the pumping structure, and the transmission line components were gathered and developed in a previous work [24], and the same models will be used in this simulation.

3.3.1 Filter Synthesis

Because the synthesis of this TVTL is not part of this thesis' work, we will be briefly going over a high-level overview of the general architecture. First off, as mentioned before, the varactor diode model used in the simulation is one extracted from a previous work [24]. After this, the pumping structure follows a double-balanced configuration as seen in the figure below:

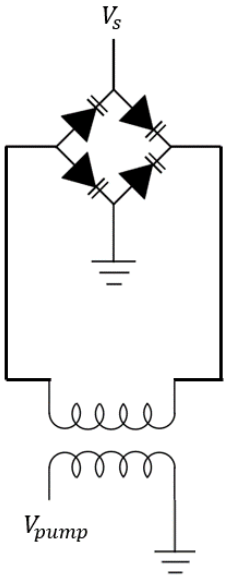

Figure 3.3.1: General double-balanced varactor diode configuration resembling that of a double-balanced mixer

For each varactor cell in the discrete TVTL structure, the pump signal is differentiated with a balun and then fed into the balanced configuration. The signal voltage is single ended in this case, and the idler voltage also feeds out into the direction of the signal voltage due to the balancing architecture. This is done to suppress the pump wave from the signal and idler path. Ideal diplexers are also added to the inputs and outputs of the TVTL structure to separate out the idler frequency (chosen to be 2.5 GHz in this case) from the signal frequency.

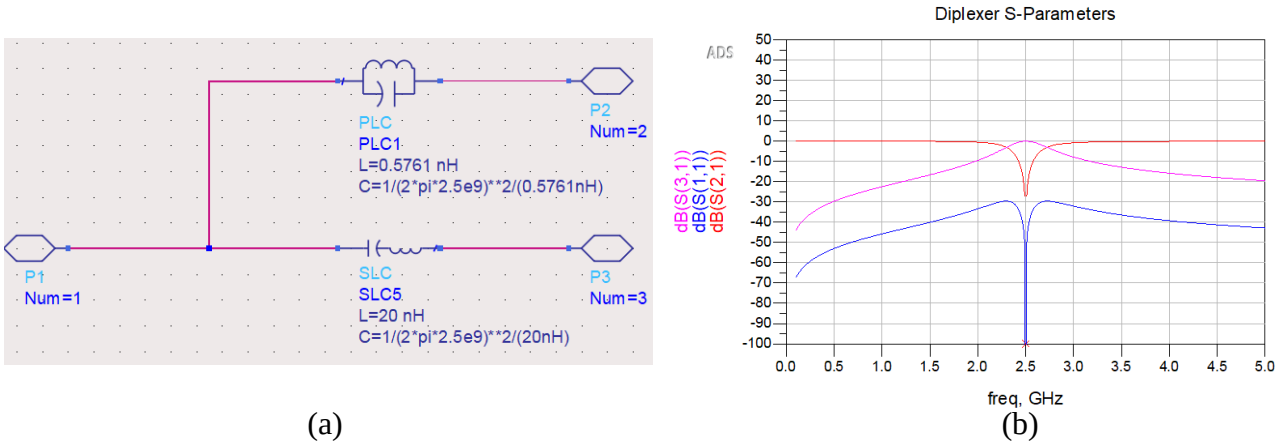

Figure 3.3.2: Ideal diplexer schematic (a) and S-parameters (b)

The final schematic of a single ideal TVTL block with 8 cells takes the following form:

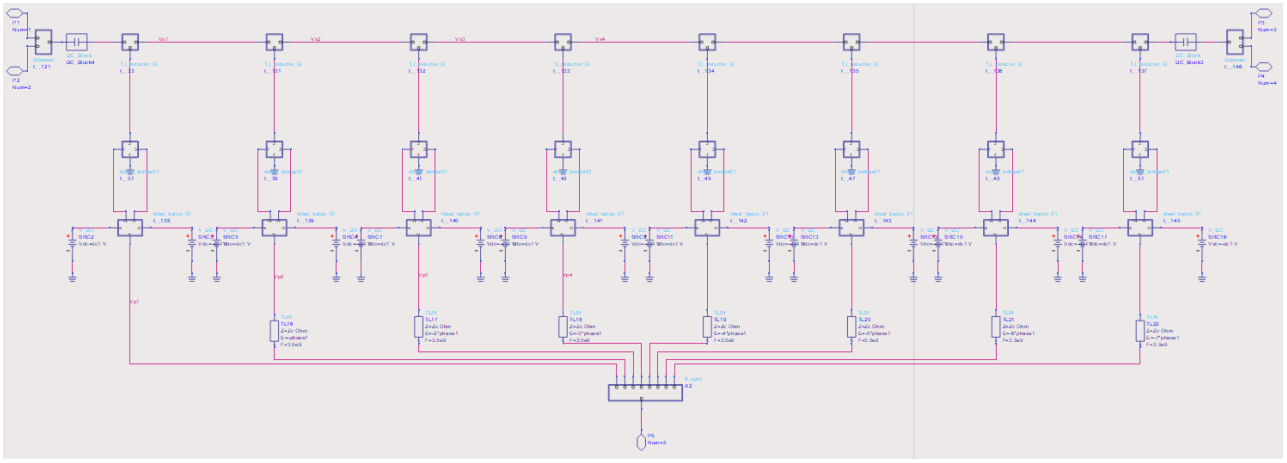

Figure 3.3.3: A single TVTL structure

As can be observed in Figure 3.3.3, the pump power is first split into 8 separate paths, with each pass having a 90 degree phase shift from the previous one. This is to mimic the traveling-wave behavior of the pump wave through the transmission line. Additionally, the transmission line is replaced with a series-inductor structure because the physical size requirement of transmission lines would not be the most space efficient from MMIC designs. The final TVTL filter in this simulation consisting of the TVTL blocks in cascade can be seen in the Figure 3.3.4 below:

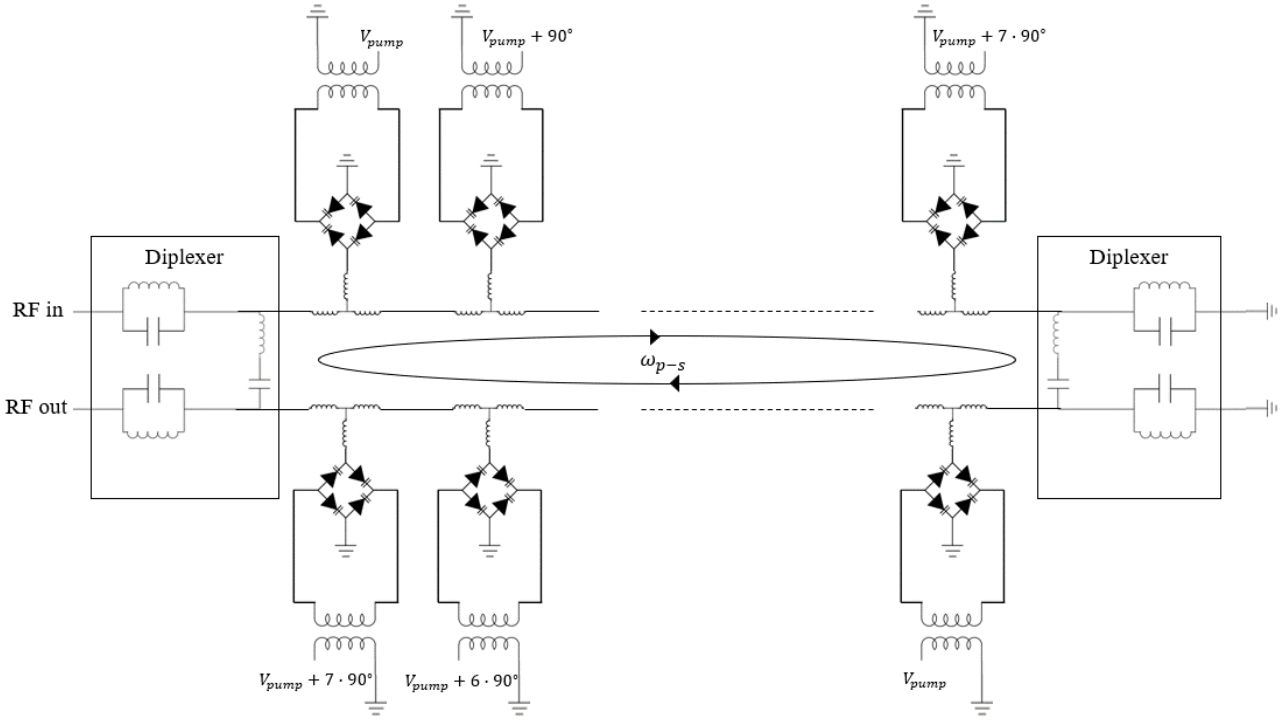

Figure 3.3.4: Full TVTL filter used for ADS simulations. For this work, the number of diode cells, N, is equal to 8 per TVTL block.

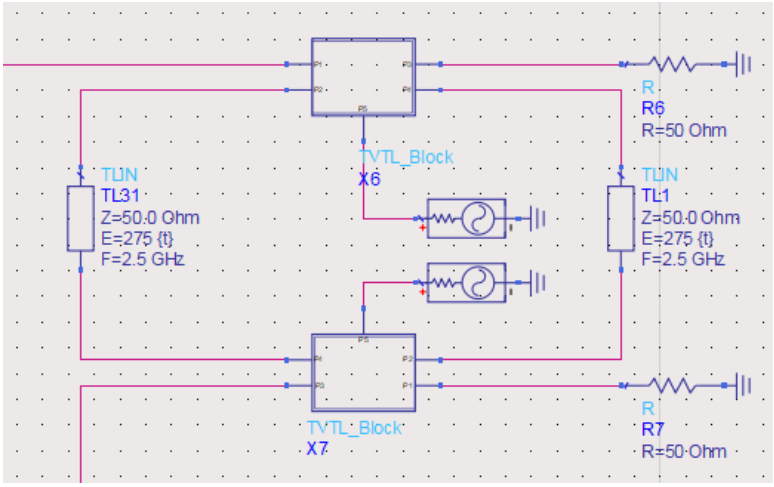

Figure 3.3.5: TVTL Filter simulation using TVTL blocks from Figure 3.3.3

3.3.2 Preliminary Simulation Results

Figure 3.3.5 highlights the simulation of the TVTL on ADS. To demonstrate the tunability of the passband, the frequency of the pump wave is swept from 3.1GHz to 3.5GHz, with a spacing of 1GHz. This should correspond to a passband sweep of 0.6GHz to 1.0GHz, which is what we observe in Figure 3.3.6 below. We also observe a roughly 60MHz bandwidth, and peak gain at the passband anywhere from 2.5 to 11dB. There is also a roughly 10dB attenuation at the out-of-band frequencies for every pump setting. This satisfies three of the conjectured points regarding the TVTL filter from before: Suppression in out-of-band frequencies, amplification in the signal frequency, and tunability of the passband frequency through altering the pump frequency. Finally, we observe in Figure 3.3.7 that the TVTL filter can most importantly function as a dynamic filter. For the simulation, the BFSK signal contains two alternating frequencies. Assuming that the time-periods in which the signal frequency switches symbols is known, we can match the pump frequency to the instances in time to pass the corresponding symbol transitions. In doing so, we also observe a preservation in charge (no re-settling period) – similar to what we observe in the theoretical dynamic filtering approach in Chapter 2.

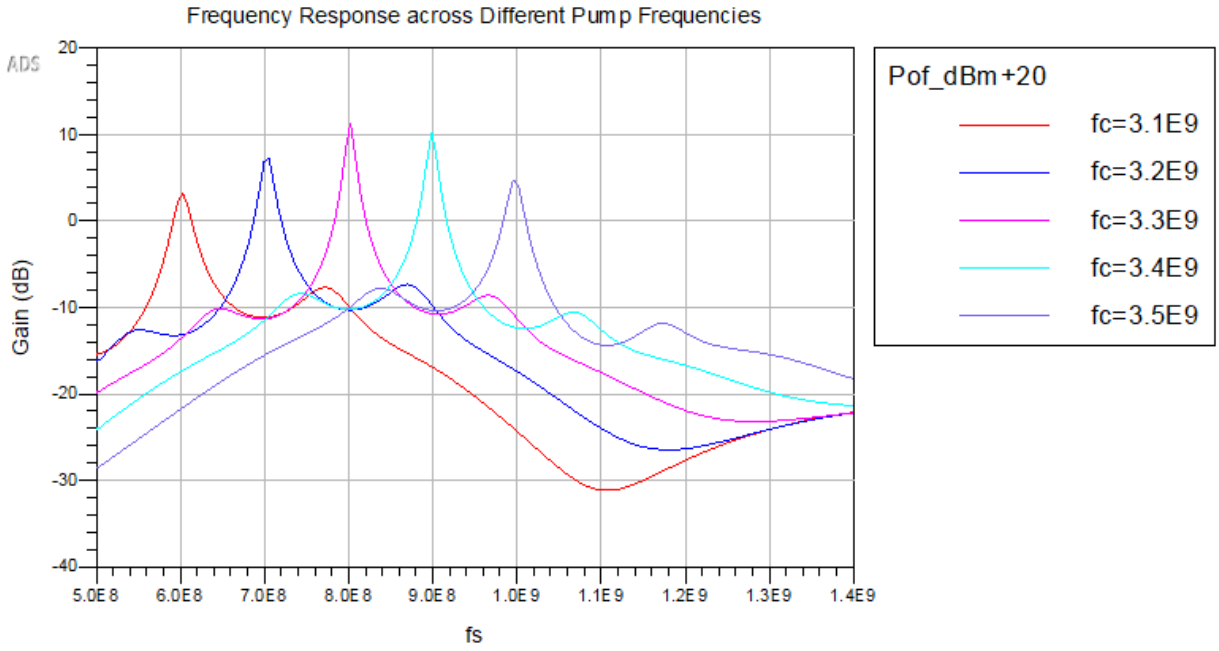

Figure 3.3.6: TVTL Filter simulation using TVTL blocks from Figure 3.3.3. The pump frequencies are swept from 3.1GHz to 3.5GHz with a 1GHz spacing, resulting in a corresponding passband frequency sweep from 0.6GHz to 1.0GHz.

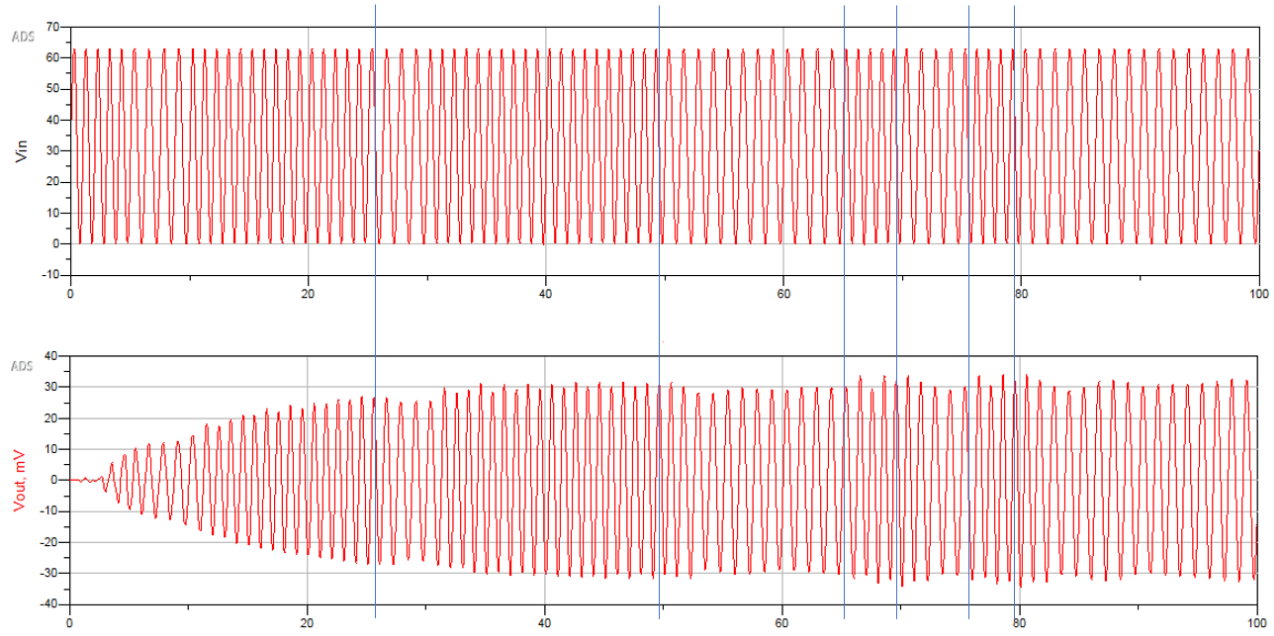

Figure 3.3.7: Dynamic Filtering of BFSK signal. Top: Input RF signal. Bottom: Output signal.

$f_0 = 0.8GHz, f_1 = 1.0GHz, BW = 200Mhz$. Symbol transitions are highlighted with a blue line.

CHAPTER 4

Front-End Leakage Suppression

As the need for wireless communications continues to grow, the availability of radio spectrum has been in even shorter supply. Typically, electromagnetic waves from a radio transmitter occupy an information channel that is divided either by time or by frequency. Because of this, interfering signals in close proximity to time-division or frequency-division channels render them inoperable. In a similar fashion, full-duplex radio systems boast the ability to simultaneously transmit and receive at the same time and frequency. Unfortunately, such systems also suffer drawbacks from the leakage of the transmitted signal into the received path, as they occupy the same channel. In this chapter, we will be exploring how the dynamic filter could be used for leakage-suppression in such communications systems.

4.1 Background on Simultaneous Transmit and Receive (STAR) System

A full-duplex system is a communications system that can transmit and receive signals at the same time and on the same frequency. This is often called a Simultaneous Transmit and Receive (STAR) radio. A perfect full-duplex link can offer twice the spectral efficiency of a half-duplex radio link because it is not constrained to solely using Time-Division Duplex (TDD) or Frequency-Division Duplex (FDD) at a given time. If such systems have an effective form of self-interference isolation, then these systems have the potential to revolutionize communication systems. However, this leads to the common problem of complicated interference due to leakage from imperfect isolation between transmitting and receiving paths. This complication can be visualized in Figure 4.1.1 below.

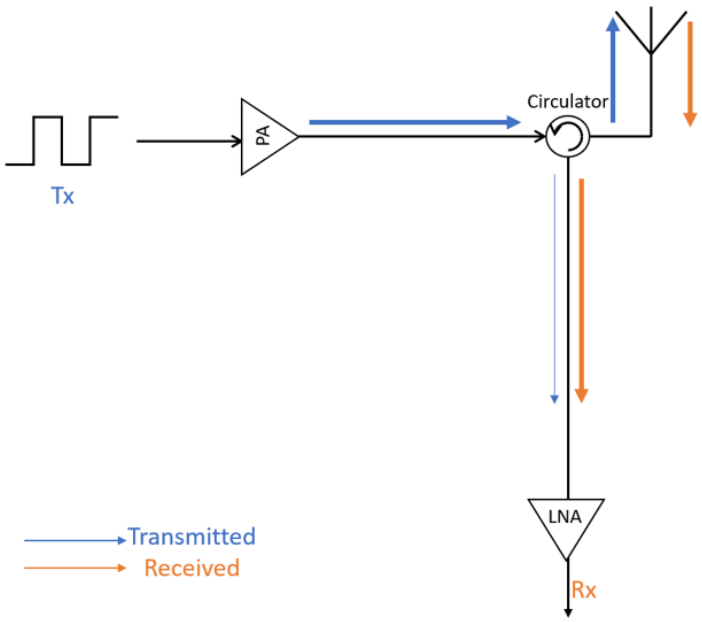

Figure 4.1.1: Traditional full-duplex communication system with a transceiver antenna. Leakage is the portion of the transmitted power which is leaked into the path designated for the received signal.

Both digital and analog implementations of leakage-cancellation structures exist for full-duplex systems to realize high isolation levels [11]-[12]. Traditionally, even within analog implementations, there are a diverse range of approaches that can be taken to achieve high isolation. A closed-loop scheme, antenna array placement, and on-chip circulators are a few examples. Typically, a more active approach involves analyzing the received signal and using that same leaked portion to cancel out its equivalent in the received signal. However, the added isolation circuitry is also usually quite complicated.

4.2 Leakage Suppression Structure

With the dynamic filter, the effectiveness of such an isolation technique increases, without the need for adaptive phase/frequency matching cancellation circuitry. In order to maximize the full potential of dynamic filters for excess noise suppression and narrow-bandwidth filtering, both the phase and frequency of the signal must be known at every single moment in time. Essentially, there must be

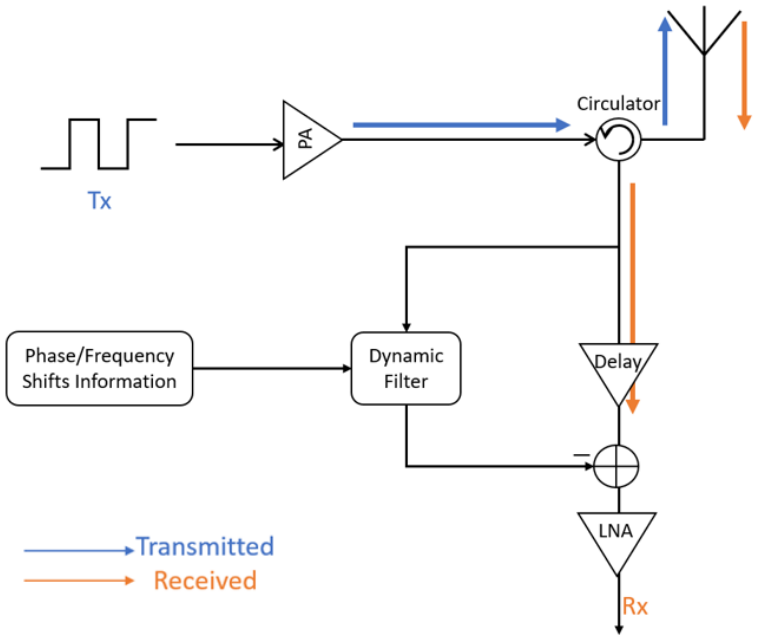

Figure 4.2.1: Schematic of front-end transceiver system using ideal dynamic filter.

knowledge on what the transmitted signal is before filtering it out, which is not usually the case. Because of this, applications maximizing the potential of dynamic filters would be limited to applications pertaining to the transmitter front-end of communications systems. Thus, an immediate application would be in the front-end of full-duplex transceiver systems for leakage suppression, in which information on the transmitted signal is presently available. This method of filtering bypasses the need for any adaptive amplitude or phase adjustment, as we are essentially filtering the exact leaked portion of the signal.

It gathers the changing frequency/phase stamps from the transmitted signal to filter the received signal with those same coefficients. That filtered signal can be used to isolate the leaked portion of the transmitted signal which makes its way through the circulator. After isolation, the phase of that isolated error signal can be flipped and then subtracted from the overall received signal before reaching the LNA. Ideally (without considering added noise), this should be able to cancel out any leakage from the transmitted signal across to the received signal.

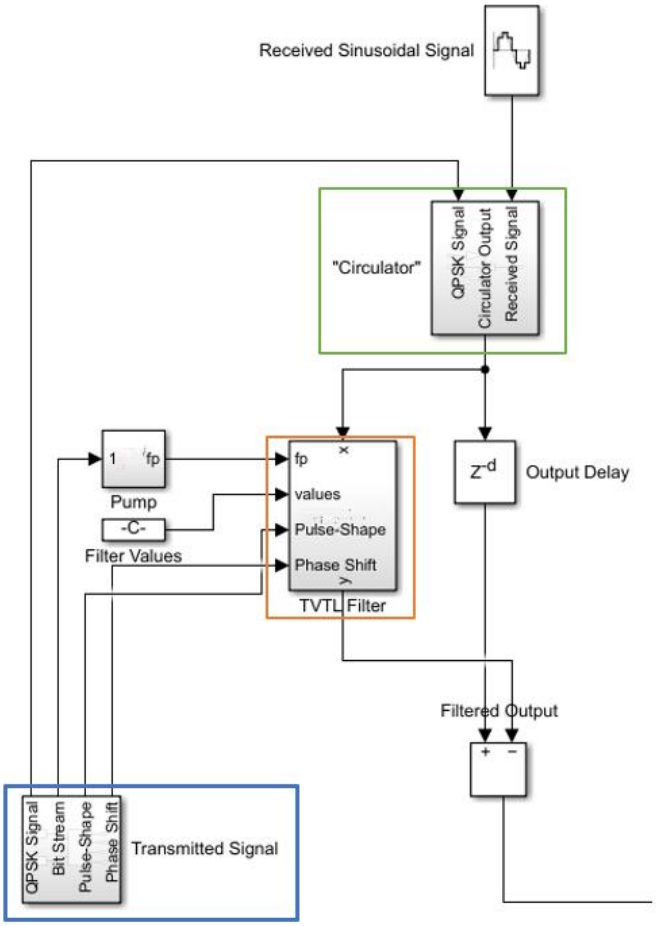

Figure 4.3.1: Simulink architecture of the leakage-suppression concept

4.3 Simulation Results

The simulation for leakage-suppression was performed with the goal of producing a theoretical limit, which would indicate whether the TVTL filtering structure would be an adequate candidate for dynamic filtering and leakage suppression. Because of this, we opted to pivot to Simulink in order to draw a more intuitive and effective diagram of the system. The Simulink diagram in Figure 4.3.1 represents the simulation architecture. This is based on the schematic in Figure 4.2.1. From the architecture, we can clearly see the same functions at work: 1) Generation of a transmitted signal (blue). 2) Imperfect isolation between transmit and receive paths (green). 3) A dynamic filter which gathers the phase/frequency shift time stamps from the transceiver (orange). The recurrence relation

derived in Equation (3.2.18) is used inside of the TVTL filter block and can be visualized in the Figure 4.3.2 below. Additionally, the phase-adjustment process is also part of this procedure.

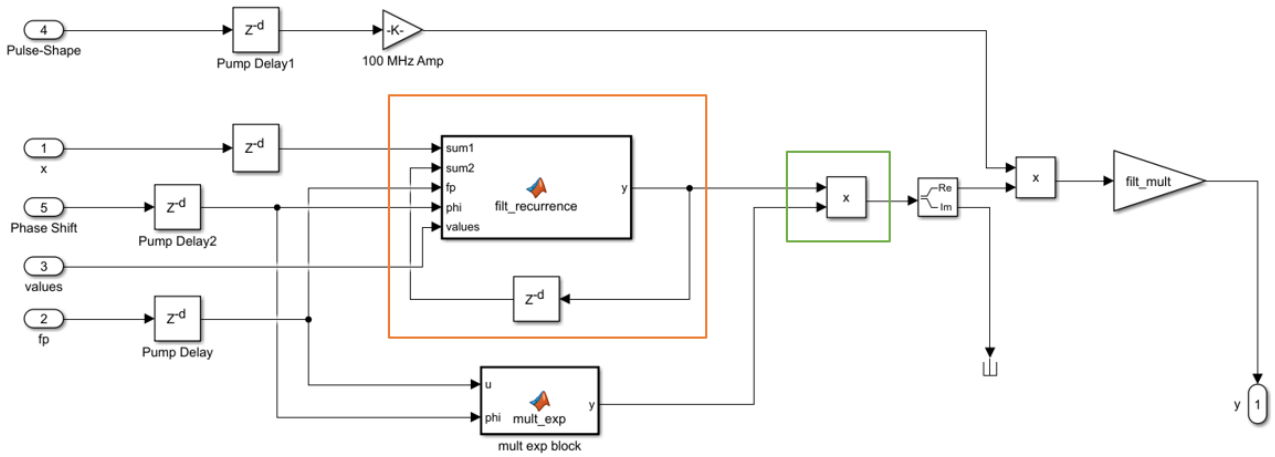

Figure 4.3.2: Simulink architecture of the TVTL filter, with Equation (3.2.18) put into realization (orange). The phase-adjustment process can be seen following the recurrence relation (green).

Finally, the QPSK-modulated signal was also pulse-shaped. This was done through first generating the bit stream, running it through a pulse-shaping filter (square root raised-cosine), and then mixing it with the phase-adjusted carrier waves.

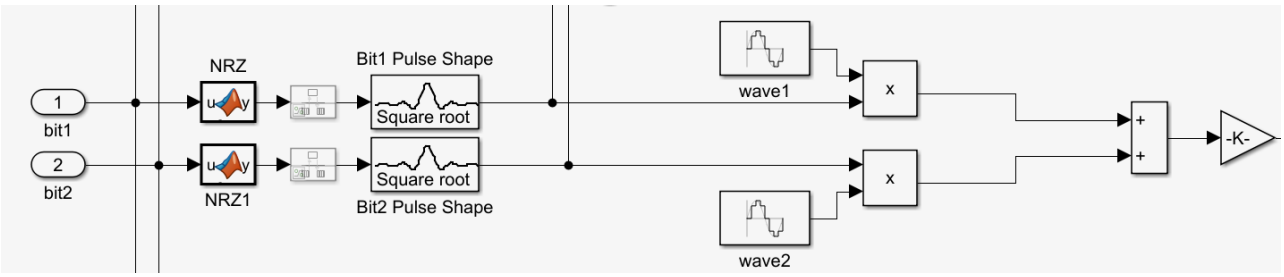

Figure 4.3.3: Pulse-shaping procedure for QPSK signal generation

Because pulse-shaping negates the discontinuities for the phase-transitions in PSK signals, the pump frequency was fed a continuous-phase information stream of the pulse-shaped signals which was tracked according to the following relation:

$$\phi = tan^{-1}\left(\frac{V_2\, sin(\delta)}{V_1 + V_2\, cos(\delta)}\right) = \tan^{-1}\left(\frac{V_2}{V1}\right) \tag{4.3.1}$$

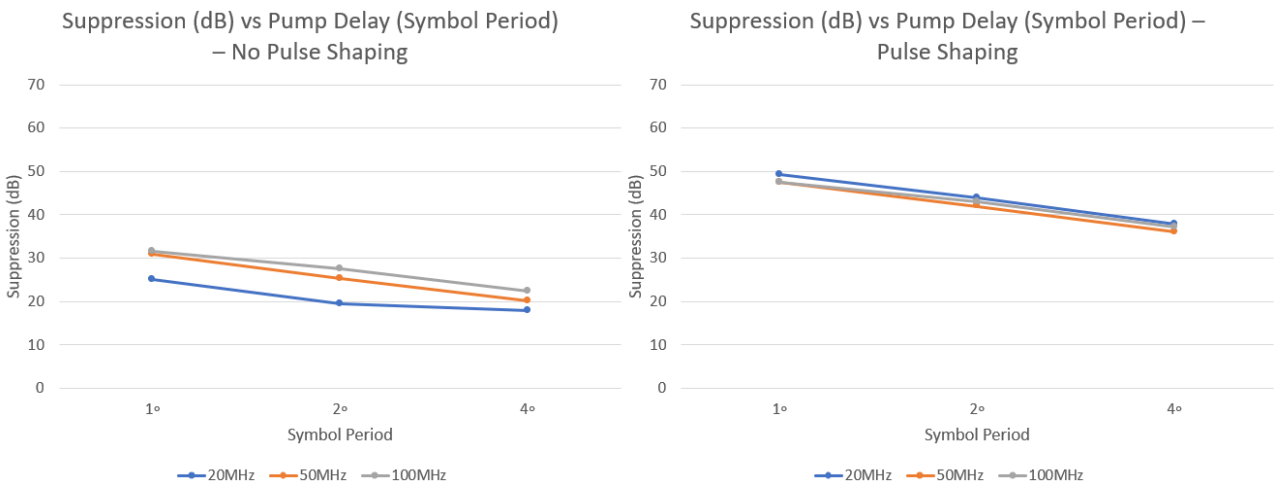

Figure 4.3.4: Theoretical suppression limits for signals with no pulse shaping (left), and signals with pulse shaping (right) with respect to the pump mismatch. The three lines correspond to three different bandwidth rates. The pump mismatch is measured with respect to the fractional degree of the symbol period.

Where V_1, V_2 are the amplitudes for the two symbol pulses. With this filtering procedure, the most important variable is the filter delay, as the received signal would have to be delayed accordingly to properly suppress the leakage. It is also the greatest cause for concern, as the concept of dynamic filtering assumes perfect passband/phase adjustments in accordance to the exact instances in time when they occur for the filtered signal. As with all systems, imperfections will exist and the delay between when the coefficients begin to switch should be accounted for. The theoretical results can be seen in Figure 4.3.4. As can be observed, with pulse-shaping this affect is not as detrimental to the system. The theoretical suppression still remains far above 30 dB (typical leakage value of a standard circulator) at a 4˚ mismatch with respect to symbol period. The effects of pulse shaping can be further analyzed in Figure 4.3.5. Visually, it is clear that symbol-transition regions are the regions which are most adversely affected by pump mismatches. However, for pulse-shaping, those are also the regions which are most attenuated due to the symbol shaping effect. The sharp discontinuous cusps are no longer as prevalent for the bottom figure (with pulse shaping) compared to that of the top figure (without pulse shaping).

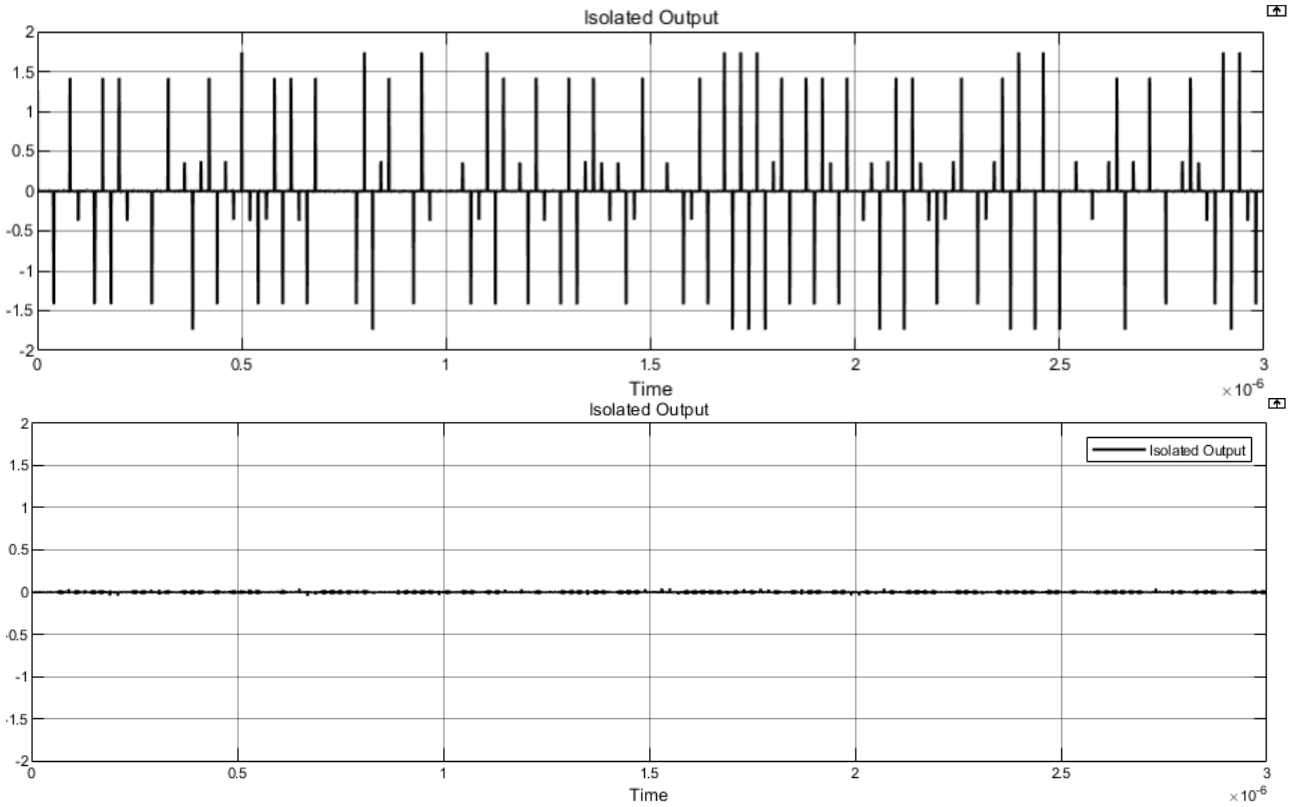

Figure 4.3.5: Suppressed leakage without pulse shaping (top), and with pulse shaping (bottom) for a 50MHz QPSK signal with 4° of pump mismatch with respect to the symbol period.

CHAPTER 5

Conclusion and Future Work

In conclusion, this work further explores the theory of complex coefficients in IIR filtering and expands the idea towards the dynamic filter – a simple way of controlling the passband and phase-adjustment of a filter while preserving the waveform. The Time-varying Transmission Line (TVTL) is not only an adequate candidate for dynamic filtering, but it also has numerous applications in the front end, such as a leakage isolator. We conclude that the fast switching, low noise, and wide frequency selectivity of such a filter would enable this type of filter to effectively cancel out transmitter-to-receiver RF leakage in a way comparable or even surpassing that of traditional methods. We also conclude that dynamic filters can be used to address some of the traditional concerns regarding spectrum utilization and rapid frequency/phase shifts. With that said, there is still much work yet to be explored with dynamic filters. Future work involves physically realizing a functional leakage-suppression prototype utilizing the TVTL filter and putting into practice the theory of dynamic filters.

REFERENCES

[1] T. Crystal and L. Ehrman, "The design and applications of digital filters with complex coefficients," in IEEE Transactions on Audio and Electroacoustics, vol. 16, no. 3, pp. 315-320, September 1968, doi: 10.1109/TAU.1968.1161998.

[2] Z. Nikolova, G. Stoyanov, G. Iliev, and V. Poulkov, "Complex Coefficient IIR Digital Filters," Digital Filters, Apr. 2011, doi: 10.5772/16041.

[3] P. Regalia, S. Mitra and J. Fadavi-Ardekani, "Implementation of real coefficient digital filters using complex arithmetic," in IEEE Transactions on Circuits and Systems, vol. 34, no. 4, pp. 345-353, April 1987, doi: 10.1109/TCS.1987.1086153.

[4] S. Nishimura and Hai-Yun Jiang, "Gradient-based complex adaptive IIR notch filters for frequency estimation," Proceedings of APCCAS'96 - Asia Pacific Conference on Circuits and Systems, Seoul, Korea (South), 1996, pp. 235-238, doi: 10.1109/APCAS.1996.569262.

[5] R. Punchalard, V. Silaphan, J. Koseeyaporn and P. Wardkein, "First order complex adaptive FIR notch filter," ECTI-CON2010: The 2010 ECTI International Conference on Electrical Engineering/Electronics, Computer, Telecommunications and Information Technology, Chiang Mai, Thailand, 2010, pp. 151-153.

[6] S. Nishimura and H. Y. Jiang, "Simplified realization of cascaded adaptive notch filters with complex coefficients," Proceedings of International Symposium on Circuits and Systems, Vol. 5, pp. 269–272, 1998.

[7] C. C. Took and D. P. Mandic, "Adaptive IIR Filtering of Noncircular Complex Signals," in IEEE Transactions on Signal Processing, vol. 57, no. 10, pp. 4111-4118, Oct. 2009, doi: 10.1109/TSP.2009.2022353.

[8] John G. Proakis and Dimitris G. Manolakis. 1992. Digital signal processing (2nd ed.): principles,

algorithms, and applications. Macmillan Publishing Co., Inc., USA.

[9] Steven W. Smith, The Scientist and Engineer's Guide to Digital Signal Processing, Second Edition, California Technical Publishing, 1999, ISBN 0-9660176-7-6

[10] R. L. Gobbi, "Intersymbol interference due to an ideal filter with linear amplitude attenuation," IEEE Conference on Military Communications, Monterey, CA, USA, 1990, pp. 1276-1280 vol.3, doi: 10.1109/MILCOM.1990.117614. Stancil, Daniel D., and Anil Prabhakar. Spin waves. Vol. 5. New York: Springer, 2009.

[11] M. Biedka, Y. E. Wang, Q. M. Xu and Y. Li, "Full-Duplex RF Front Ends : From Antennas and Circulators to Leakage Cancellation," in IEEE Microwave Magazine, vol. 20, no. 2, pp. 44-55, Feb. 2019, doi: 10.1109/MMM.2018.2880496.

[12] P. D. L. Beasley, A. G. Stove, B. J. Reits and B. As, "Solving the problems of a single antenna frequency modulated CW radar," IEEE International Conference on Radar, Arlington, VA, USA, 1990, pp. 391-395, doi: 10.1109/RADAR.1990.201197.

[13] P. Sutthikarn, S. Chivapreecha, T. Jongsataporn and A. Trirat, "Tunable Bandpass/Bandstop Digital Filters Basedon 1st-order Allpass Network Instead of Unit Delay," 2019 5th International Conference on Engineering, Applied Sciences and Technology (ICEAST), Luang Prabang, Laos, 2019, pp. 1-4, doi: 10.1109/ICEAST.2019.8802574.

[14] H. K. Kwan, "Tunable and variable passive digital filters for multimedia signal processing," Proceedings of 2001 International Symposium on Intelligent Multimedia, Video and Speech Processing. ISIMP 2001 (IEEE Cat. No.01EX489), Hong Kong, China, 2001, pp. 229-232, doi: 10.1109/ISIMP.2001.925374.

[15] S. Chivapreecha, "Universal biquadratic digital filter with tunable capability," TENCON 2011 - 2011 IEEE Region 10 Conference, Bali, Indonesia, 2011, pp. 720-724, doi: 10.1109/TENCON.2011.6129203.

[16] B. Boashash and M. Mesbah, "Signal enhancement by time-frequency peak filtering," in IEEE Transactions on Signal Processing, vol. 52, no. 4, pp. 929-937, April 2004, doi: 10.1109/TSP.2004.823510.

[17] J. Náhlík, J. Hospodka, P. Sovka and B. Přenička, "Switched capacitor circuit implementation of two-channel filter bank," 2013 International Conference on Applied Electronics, Pilsen, Czech Republic, 2013, pp. 1-4.

[18] S. F. Peik, B. Jolley and R. R. Mansour, "Switched superconductive filter-banks," 2004 IEEE MTT-S International Microwave Symposium Digest (IEEE Cat. No.04CH37535), Fort Worth, TX, USA, 2004, pp. 131-134 Vol.1, doi: 10.1109/MWSYM.2004.1335821.

[19] I. C. Reines et al., "A low loss RF MEMS Ku-band integrated switched filter bank," in IEEE Microwave and Wireless Components Letters, vol. 15, no. 2, pp. 74-76, Feb. 2005, doi: 10.1109/LMWC.2004.842823.

[20] X. Yang, M. Xing, E. Wang, L. Zhang, N. Li and Z. Qian, "A design of S-band monolithic integrated switched filter bank," 2017 18th International Conference on Electronic Packaging Technology (ICEPT), Harbin, China, 2017, pp. 177-181, doi: 10.1109/ICEPT.2017.8046433.

[21] Y. E. Wang, "Non-reciprocity with time-varying transmission lines (TVTLs)," 2012 IEEE International Conference on Wireless Information Technology and Systems (ICWITS), 2012, pp. 1-4, doi: 10.1109/ICWITS.2012.6417737.

[22] S. Qin and Y. E. Wang, "A nonreciprocal, frequency-tunable notch amplifier based on Distributedly Modulated Capacitors (DMC)," 2016 IEEE MTT-S International Microwave Symposium (IMS), 2016, pp. 1-3, doi: 10.1109/MWSYM.2016.7540316.

[23] X. Zou, Q. Wu and Y. E. Wang, "Monolithically Integrated Parametric Mixers with Time-varying Transmission Lines (TVTL)," 2019 IEEE MTT-S International Microwave Symposium (IMS), 2019, pp. 971-974, doi: 10.1109/MWSYM.2019.8700793.

[24] X. Zou, “Monolithically Integrated Time-Varying Transmission Lines (TVTL) for Tunable and Interference Resilient RF Front Ends,” Ph.D. dissertation, ECE, UCLA, Los Angeles, CA, 2021.

[25] S. Qin, Q. Xu and Y. E. Wang, "Nonreciprocal Components With Distributedly Modulated Capacitors," in IEEE Transactions on Microwave Theory and Techniques, vol. 62, no. 10, pp. 2260-2272, Oct. 2014, doi: 10.1109/TMTT.2014.2347935.

[26] P. K. Tien and H. Suhl, "A Traveling-Wave Ferromagnetic Amplifier," in Proceedings of the IRE, vol. 46, no. 4, pp. 700-706, April 1958, doi: 10.1109/JRPROC.1958.286770.

[27] Tien, P. K. "Parametric amplification and frequency mixing in propagating circuits," J. Appl. Phys., vol. 29, no. 9, pp. 1347-1357, Sep. 1958.

[28] Q. Wu, X. Zou, R. Zhu and Y. E. Wang, "Chip-Scale RF Correlator with Monolithically Integrated Time-Varying Transmission Line (TVTL)," 2018 IEEE/MTT-S International Microwave Symposium - IMS, Philadelphia, PA, USA, 2018, pp. 431-434, doi: 10.1109/MWSYM.2018.8439846.

[29] Y. E. Wang, "Time-varying transmission lines (TVTL) - A new pathway to non-reciprocal and intelligent RF front-ends," 2014 IEEE Radio and Wireless Symposium (RWS), Newport Beach, CA, USA, 2014, pp. 148-150, doi: 10.1109/RWS.2014.6830149.